EMBRITTLEMENT OF ZINC CRYSTALS BY MERCURY

by

JYUNG-HOON KIM

A THESIS SUBMITTED IN PARTIAL FULFILMENT

OF THE REQUIREMENTS FOR THE DEGREE OF

MASTER OF APPLIED SCIENCE

IN THE DEPARTMENT

OF

METALLURGY

We accept this thesis as conforming to the

standard required from candidates for

the degree of MASTER OF APPLIED SCIENCE

THE UNIVERSITY OF BRITISH COLUMBIA

January, 1966.

In presenting this thesis in partial fulfilment of the requirements for an advanced degree at the University of British Columbia, I agree that the Library shall make it freely available for reference and study. I further agree that permission for extensive copying of this thesis for scholarly purposes may be granted by the Head of my Department or by his representatives. It is understood that copying or publication of this thesis for financial gain shall not be allowed without my written permission.

Department of Metallurgy

The University of British Columbia,
Vancouver 8, Canada

Date February 15th, 1966

THE UNIVERSITY OF BRITISH COLUMBIA

VANCOUVER 8, CANADA

DEPARTMENT OF METALLURGY

February 11th, 1966.

COMMENTS ON THESIS

"Embrittlement of Zinc Crystals by Mercury"

by Jyung-Hoon Kim

At the oral presentation held in the Department of Metallurgy on Wednesday, January 26, 1966, it was decided that the thesis should be accepted, but with the following comments:

1. The quality of the English composition is well below the usual standard normally expected of students whose native language is English. However, by majority opinion, it was agreed that in a case where English is not a student's mother language, it is preferable that the thesis be written in imperfect English and represent the student's own writing and thinking, than to have perfect English arising from extensive rewriting or revision by the supervisor. The overriding consideration, however, must be that the thesis shall be sufficiently well written to avoid any ambiguity of thought or misstatements of fact.

2. It was felt that some of the detailed conclusions expressed in this thesis were unwarranted by the nature of the results. However, it was felt that this could be due, in part, to the language problem, and that in any case, the quality of the work generally warranted its acceptance.

ABSTRACT

A study has been undertaken to investigate the loss of ductility and modified work hardening characteristics of zinc single crystals coated with mercury.

Important results of tensile tests performed under fixed experimental conditions are summarized to be:

(1) increase in critical resolved shear stress, and increase of work hardening slope in stage A and stage B

(2) decrease in transition strain from stage A to stage B

(3) decrease in fracture stress and fracture strain.

The results have been interpreted in the context of the present understanding of deformation theory of C.P.Hex. metals.

In addition, relevant mechanisms for crack initiation have been studied with the aid of microscopic observations of deformed crystals.

ACKNOWLEDGEMENT

The author gratefully acknowledges the guidance of Dr. E. Teghtsoonian, the director of this research.

He wishes to thank the members of the faculty and fellow graduate students of the Department of Metallurgy for their continued support and interest in this work.

Special thanks are extended to Mr. R. Richter for assistance with equipment and Mr. R. G. Butters for technical advice.

The author is grateful for financial assistance provided by the Research Corporation, New York, the National Research Council of Canada, and Canadian Western Pipe Mills of Port Moody, B.C.

TABLE OF CONTENTS

Table of Contents (cont'd)

Table of Contents (cont'd)

LIST OF FIGURES

List of Figures (cont'd)

LIST OF TABLES

I INTRODUCTION AND REVIEW OF THE LITERATURE ON EMBRITTLEMENT BY LIQUID METALS

A. INTRODUCTION

The effects of surface environment on the plastic deformation of materials have been observed for many years. According to various investigations, the materials influenced range from stone and glass to pure metals and alloys in environments which are either gases or liquids.

Many investigators have attacked this field under a variety of headings such as stress corrosion, hydrogen embrittlement, corrosion fatigue, liquid metal corrosion and fatigue.

There are many similarities evident in all of the topics just mentioned. However, in this paper, particular attention will be focussed on those investigations relating to liquid metal embrittlement.

The effect of surface active media on the mechanical behavior of materials has been studied extensively in the Soviet Union since the early work of Rehbinder in 1931. Liquid metal embrittlement was considered within the broad field of physicochemical mechanics whereby the surrounding media modify the physical and mechanical properties of materials as a result of the formation of adsorbed surface layers. Possible surface active media can be solid, liquid or gaseous. The main effect of such a layer is to reduce the strength and hardness of the material with increased ductility.

In considering liquid metal embrittlement, we usually observe drastic decrease in ductility. Also the role of dislocation can not be over-

looked because some plastic deformation always precedes embrittlement by liquid metals. Any dislocation mechanism for crack initiation presupposes some stable obstacles to the motion of dislocations. With polycrystalline materials, this function is usually performed by a grain boundary. However it has been observed that, in some material, cracks may be initiated in the center of grains[1]. Studies on single crystals, particularly cadmium[2], have provided good evidence that both crack initiation and propagation can be assisted by the presence of active liquid metal atoms. Therefore it is quite conceivable that liquid metal environments either provide a barrier or stabilize some potential barrier to dislocation movement.

B. REVIEW OF THE LITERATURE ON EMBRITTLEMENT BY LIQUID METALS

(i) The Effect of Liquid Metal on the Plastic Deformation of Polycrystalline Materials

The loss of strength and ductility of metals under stress and in contact with surface active metals has been the subject of many investigations. Reported results indicate disagreement on the nature of the embrittlement and principal mechanisms involved reflecting the complexity of the problems related with liquid metal embrittlement.

To develop the picture that both stress and liquid metals are necessary conjointly for the initiation of embrittlement, Heyn[3], Rawdon[4], and Moor and Beckinsale[5] have done experiments with brass wetted by mercury. It was their belief that the simultaneous effects of internal stresses in the material and the penetration of mercury deposited at the grain boundaries of

the brass caused intergranular cracking.

Investigation of elevated temperature effects permitted the use of a wide range of liquid metals in addition to mercury. Miller[6] determined the tensile properties of 60/40 and 70/30 brasses coated with liquid tin, lead, and solder at temperature up to 350°C, and found the embrittlement process was similar to that of brass by mercury although high stresses were required for fracture.

Recently, Rosenberg and Cadoff[7] pointed out that the wide variation in results were due to the wide variety of experimental programs carried out, and focussed intensive attention to a detailed study of one system, copper alloys, wetted with mercury and mercury base solutions. They came to following conclusions:

(1) The elongation of copper in mercury is greater than that of the Cu-Zn alloy, the latter being generally considered a case of embrittlement.

(2) The effect of grain size on yield strength, fracture strength, and loss of elongation are to be noted. The relationship between fracture stress τ_f versus grain size, $D^{-1/2}$ can be related by

$$\tau_f = \tau_{0f} + K_1 D^{-1/2} \qquad \ldots\ldots 1$$

where τ_{0f} and K_1 are constants of the system.

(3) The fracture characteristics of copper-aluminum, copper-gold, and copper-germanium alloys wet with mercury are similar to those described for the copper-zinc system. The susceptibility to embrittlement for all four systems is in the order zinc < aluminum < germanium < gold.

(4) In copper-zinc system, the relation between the yield stress τ_{ys} and the grain size $D^{-1/2}$ is given by

$$\tau_{ys} = \tau_{oy} + K_2 D^{-1/2} \quad \ldots\ldots 2$$

where τ_{oy} and K_2 are constants of system.

(5) The wetting action associated with changing the liquid-metal composition is reintroduced as a significant variable. The concepts of surface energy alone do not appear to explain the wide variation (an increase in fracture stress over that obtained in pure mercury) caused by changes in the liquid-metal composition. The interaction of liquid metal with the solid at the root of the stabilized or advancing crack is necessary for a complete understanding of the problem.

(6) The grain size dependence observed in the prestrain experiments indicates that, for large grain samples, the dislocation pile-up dependence on grain diameter controls the fracture and thus there is greater susceptibility at larger grain sizes.

(7) The measurements for fracture boundaries appear to be somewhat scattered at first glance, but closer inspection shows that the angle between slip planes in adjacent grains is not of major significance, that only coincidence of slip direction is necessary for the inhibition of mercury penetration.

(ii) <u>The Effect of Liquid Metal on the Plastic Deformation of Single Crystals</u>

Likhtman and Shchukin[8] investigated the effect of a mercury coating on the deformation characteristics of zinc single crystals. The crystals of orientation $X_o = 48°$ were tested at room temperature. (X_o = angle between

tensile axis and slip plane). They found that the shear stress and shear strain at fracture were respectively reduced from 140Kg/cm^2 and 260% in air to 20Kg/cm^2 and 10% in mercury.

Shchukin et al[9] studied the orientation dependence of normal stress at fracture τ_F and shear strain at fracture γ_F for amalgamated zinc single crystals. They established a criterion for the brittle fracture which approximates the constancy of the product of normal and cleavage stress relative to the basal plane of differently oriented zinc monocrystals. This constancy is expressed by

$$\tau_F \gamma_F = K^2 \qquad \ldots\ldots 3$$

where $K = k (G\gamma/L)^{1/2}$, k being a dimensionless constant of order unity, G the shear modulus, γ the specific free energy and L the length of slip plane.

The effect of temperature and alloy liquid metals with various concentration were investigated by Rehbinder, Kochanova, Bryukhanova and Labzin[10-12]. Zinc single crystals in the form of 0.5mm wire were coated with tin, lead, alloys of tin and lead in various concentration, and mercury. With tin-coated zinc crystals tested in tension at a temperature below the melting point of the Zn/Sn eutectic, a slight increase in tensile strength was observed. At higher temperature (350° and 400°C) the strength and ductility decreased remarkably. Also at the same temperature the nature of fracture changed from a ductile type (uncoated) to a brittle type (coated with liquid tin). Both the fracture stress and elongation were reduced. This

was considered to be related with:

(1) An increase in the solubility of zinc in liquid tin as the temperature was raised from 350 to 400 °C.

(2) A corresponding decrease in the interface surface tension.

However, Kamdar and Westwood[13] pointed out the fact that the Russian work did not include an interpretation involving the existence or nature of stable obstacles to the motion of dislocations. They paid special attention to the object of revealing the nature of any suitably stable obstacles to slip. For this purpose, the behavior of amalgamated single and asymmetric bicrystals were carefully studied. They classified the single crystals into three groups based on X_o, the angle between specimen axis and the (0001) basal plane.

In group I where $X_o < \sim 15°$, crystals were deformed principally by twinning and both partially amalgamated and chemically polished specimens failed after only a few percent strain by secondary cleavage on the (0001) planes of a twin. It was suspected that, under certain circumstances, twin boundaries would serve as stable barriers to dislocation motion. To examine this hypothesis, they introduced twins into crystals of orientation $X_o = 25°$ and 45° by gently indenting the crystals with the blunt end of a needle. Then oxide free specimens were amalgamated in the vicinity of twins and lightly strained. Cleavage cracks were observed to initiate at twin boundary and to propagate along basal planes of the matrix crystal.

In group II where $15° < X_o < 70°$, partially amalgamated crystals deformed in a ductile manner and did not fracture until shear stresses of the order 600-1000g/mm^2 and strains of order 125-250% were attained. Fracture of both partially coated and uncoated crystals eventually occurred after repeated twinning and usually by secondary cleavage on the (0001) plane of a twin. Occasionally, amalgamated specimens did fracture at relatively low strains (20-60%) and examination of these specimens revealed that, in all instances, fracture had initiated at kink bands which formed in the vicinity of the grips during the tensile test.

In group III where $X_o > 70°$, crystals were significantly embrittled by mercury and fracture occurred always at a kink band formed in the amalgamated gauge section.

They carried out further experiments with partially amalgamated asymmetric bicrystals and found that cleavage cracks were initiated at the grain boundary of bicrystals, and propagated completely through the crystals.

Their conclusions can be summarized as follows:

(1) Adsorption of the liquid metal at some stable obstacle to slip is a necessary condition of liquid metal embrittlement. Consequently, zinc single crystals oriented for single slip and tested in tension are not embrittled unless the liquid metals are adsorbed specifically at kink bands formed near the grips during deformation.

(2) Experiments with amalgamated bicrystals provide convincing support for cleavage fracture in zinc proposed by Likhtman-Shchukin and derived from an analysis by Gilman.

The effect of mercury on the cleavage fracture energy of zinc single crystals was also investigated by Westwood and Kamdar[14]. They applied Obreimov-Gilman cleavage technique in which partial crack was introduced by crack initiating jig and prevented from propagating completely through the specimen by the application of a small compressive stress perpendicular to the direction of propagation. They found the total energy involved in the propagation of a crack, ϕ can be expressed by the relation

$$\phi = \eta \rho \gamma_o \qquad \ldots\ldots 4$$

where η is the coefficient of embrittlement which relates the energy required to separate atoms at crack tip in the presence and absence of mercury, ρ is a dimensionless variable depending upon the degree of plastic relaxation at the crack tip and independent of η, and γ_o is the true surface energy of the fracture plane. In their work $\gamma_{o_{Zn(298°K)}}$ was determined to be 87 ± 5 erg/cm^2 and $\eta_{Zn\text{-}Hg(298°K)}$ to be 0.61 ± 0.12.

(iii) Survey of Embrittlement Couples

Pertsov and Rehbinder[15] have studied embrittlement couples with the aid of binary phase diagram. They found semiempirical rules indicating whether or not a given molten metal M_1 is strongly surface active in regard to another metal M_2 of higher melting point. Their results can be summarized as follows: (see Table I).

(1) There is considerable reduction in strength and ductility if metal M_1 has a narrow, but finite, region of solubility in the solid state in the metal M_2.

(2) On the contrary, no embrittlement effect is normally observed if this solubility region is very wide or absent altogether.

TABLE I

Embrittlement Couple

Reduction in strength of metal under the effect of a molten metal coating		No reduction in strength of metal under the effect of a molten metal coating	
Metal Studied	Metal Coated	Metal Studied	Metal Coated
Cadmium	Tin	Cadmium	Mercury
Cadmium	Gallium	Lead	Mercury
Zinc	Mercury	Copper	Mercury
Zinc	Gallium	Copper	Tin
Zinc	Tin	Copper	Zinc
Tin	Mercury	Zinc	Lead
Tin	Gallium	-	-
Copper	Bismuth	-	-

C. THE AIM OF PRESENT INVESTIGATION

Although various kinds of experiments on liquid metal embrittlement have been carried out to establish the exact mechanism and associated problems, none of them paid special attention to the work hardening characteristics of single crystals in the presence of surface active media.

In this present investigation, an attempt has been made to explain the liquid metal embrittlement in the context of the present understanding of deformation theory under the following experimental schemes.

(1) The system studied consists of zinc single crystals of fixed orientation wetted by mercury as a surface active metal.

(2) The amount of mercury used for coating and time of immersion of crystals in mercury were fixed.

(3) Critical resolved shear stress τ_c, work hardening slope in stage A (θ_A) and stage B (θ_B), transition strain from stage A to B, γ_{A-B}, fracture strain γ_f and fracture stress τ_f were defined as parameters to compare the results obtained from different experimental conditions.

Critical resolved shear stress was determined from the stress at which the shear stress strain curve first deviates from linearity because coated specimens under certain experiment conditions fail before the full development of stage A making assessment of the value τ_c by extrapolating stage A impossible.

II. EXPERIMENTAL PROCEDURE

A. MATERIAL

The zinc used in this experiment was purchased from the Consolidated Mining and Smelting Company Limited, Trail, B.C., Canada. The purity of the zinc was 99.999 +%.

Commercial grade of mercury was treated with concentrated mercuric nitrate and oxidized so that base metal impurities can be removed. The mercury used in this experiment was mainly contaminated by zinc, solder (specimen mounting alloy), and aluminum (grip). During the oxidation, a silvery froth begins to form and agitators continually force the froth through the mass of mercury. The froth darkens and thickens to a layer. As the oxidation proceeds further, a black powder forms on the surface and the froth gradually disappears, leaving a layer of dry, black powder floating on bright mercury. Oxidized mercury was filtered by mercury filter which consists of a reservoir with discharge aperture at the bottom. Surrounding this aperture is a ring of gold, which is the filtering element. Finally mercury is filtered by gold adhesion principle. Contaminated mercury from wetting of zinc crystals is purified using the above mentioned method.

B. SPECIMEN PREPARATION

(i) Growth of Single Crystals

The single crystals were grown from melt by Bridgman's method. Extruded zinc wire together with seed crystal was charged into pyrex glass tube which has a closed sharp tip at one end. The other end of the pyrex

mould was connected to vacuum pump to evacuate air in it and sealed off to prevent oxidation of zinc during growth. The furnace used for growing crystals is a vertical type with Ni-Cr wire as heat element. A thermocouple was inserted halfway of the furnace body and the temperature was controlled by WHEELCO type controller. The temperature in the vicinity of the thermocouple was 450°C. The vertical travelling rate of the charged mould in the furnace was 35 mm/hr. After determining temperature distribution of the furnace, the upper half of the seed crystal was placed at melting zone so that the melt of polycrystalline zinc would turn into monocrystal as the charge moves down. Four charged pyrex molds were treated as a single batch by above mentioned technique and as a result, four long crystals of about 40cm long were obtained at one time. To remove the crystals from the mould without introducing undesired deformation, the glass mould was dissolved in 48% HF solution. The thin oxide film formed during growth kept crystals from attacking by HF solution.

Back-reflection Laue X-ray method was applied to determine the orientation of the grown crystals. The orientation of all crystals used in this investigation was $X_o = 46° \pm 3°$ and $\lambda_o = 46° \pm 4°$, where X_o is the angle between the specimen axis and slip plane, and λ_o is the angle between the specimen axis and slip direction. This orientation is such that slip system operates along (0001) plane in the direction of $[11\bar{2}0]$.

(ii) Surface Coating of the Single Crystals with Mercury

The specimens were polished by electropolishing technique in the mixture solution of 25g Cr_2O_3, 7cc H_2O and 133cc Conc. CH_3COOH.

On removing oxide film on the surface, the crystal was mounted in aluminum grips with solder. Ordinary soldering flux pasted at the end of the crystal improved wetting of crystals with molten solder. MICROSTOP covered the exposed solder at the grip to avoid contact between mercury and solder. Then both ends of mounted crystal were wrapped with polyethylene paper to reduce the possibilities of early failure resulting from adsoption of mercury at the kink that appears frequently in the vicinity of grip during deformation. The mounted crystal with protected ends was placed in a stainless steel jig horizontally and tightened very carefully by using two arms stretched out of the middle of the jig. Finally, the jig was immersed into fixed amount of clean mercury contained in a plastic boat, and the time of immersion was measured by stop watch. Fig. 1 shows the mounting apparatus and stainless steel jig which holds mounted specimen. The dimensions of a mounted specimen are shown in Figure 2.

C. TENSILE TESTING

A screw driven INSTRON tensile testing machine was used for the test. The universal gripping heads were mounted below the cross head so that water bath can be attached in the high temperature test. The gimbals grips which have two rotational axis were used to achieve quick and smooth alignment of specimen to the tension axis. The strain rate and chart speed were fixed as 0.1"/min and 1.0"/min respectively. The tensile test results were recorded by autographic recorder in the form of load-elongation curve. CT and C cell were used and before proceeding every test, the load system was calibrated to obtain correct load applied to specimens.

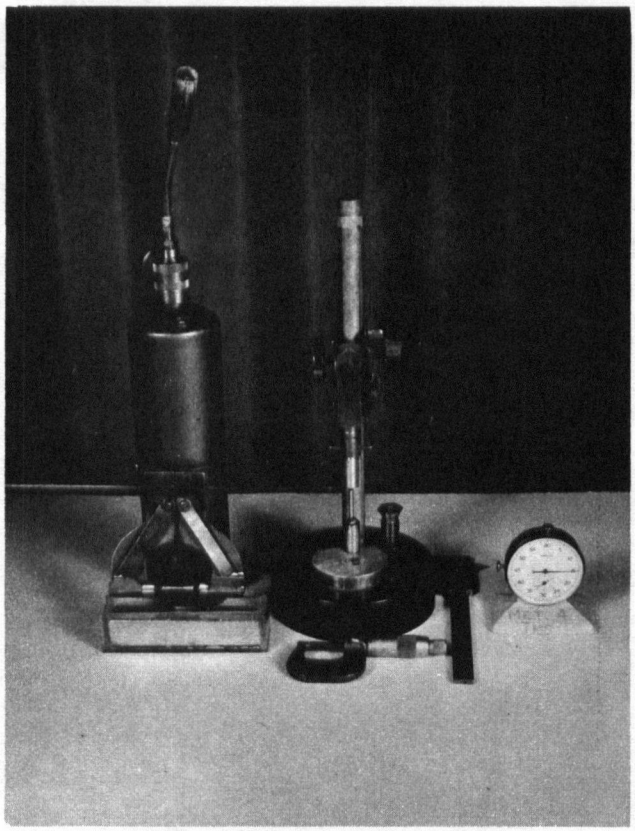

Fig. 1. Mounting Apparatus and Jig.

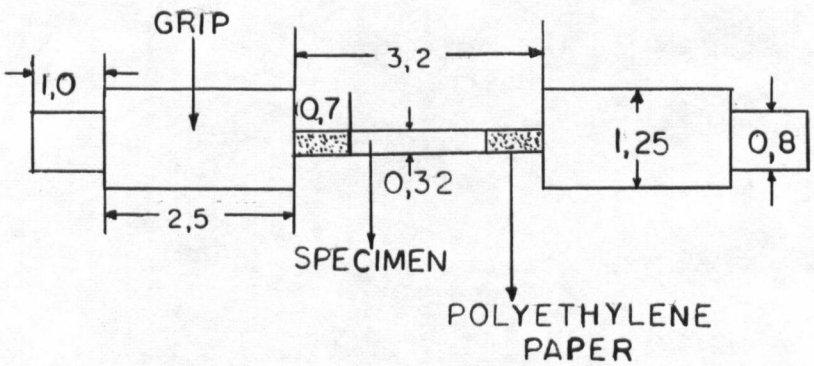

Fig. 2. Dimensions of Mounted Crystal. (Unit: cm)

III. EXPERIMENTAL RESULTS

A. WETTING EXPERIMENT

(i) Zn-Hg System

The phase diagram of Zn-Hg system determined by E.A. Anderson[16] is shown in Fig. 3.

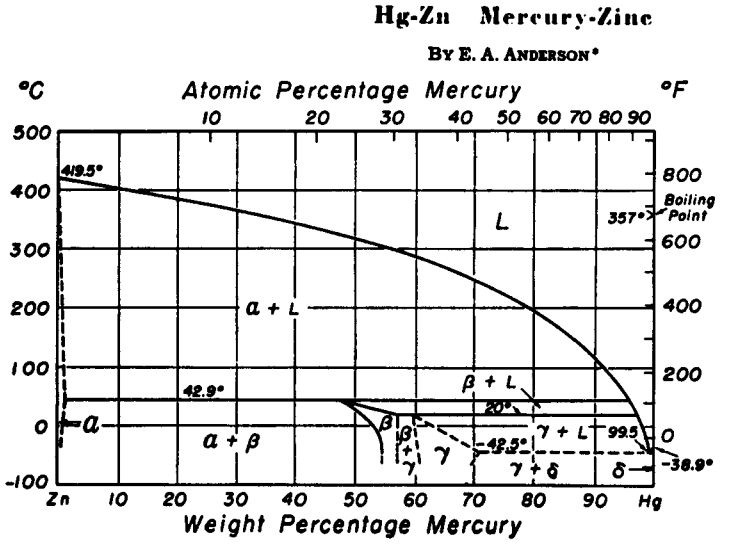

Fig. 3. Hg-Zn System (from Metals Handbook)

The solubility of mercury in solid zinc has not been established accurately, but is probably less than 1% at room temperature. According to Von Simson[17] the β phase is hexagonal with an axial ratio of 2.01. The crystal structure of δ phase, stable only below room temperature, has not been determined.

(ii) Wetting Experiment with Polycrystalline Zinc

Mercury is strongly surface active with respect to zinc. As a first step to establish the relation applying to the wetting of mercury over the surface of zinc, two groups of polycrystalline zinc specimens with different grain size were prepared by extrusion at two different temperatures. Each specimen of the same group had the same dimension. On polishing the surface, each specimen was wetted in 10cc clean mercury and time of immersion was recorded by stop watch.

The weight gained per unit surface area of the specimen was determined by taking the weight difference between wetted and unwetted specimen and dividing it by total surface area. The result is given in Fig. 4. The specimens of small grain size (90μ) revealed a maximum at 130 secs with the weight gained, 1.05mg/cm^2. On the other hand, the maximum weight gained by specimens of larger grain size (190μ) was shifted to left with the value of 2.66mg/cm^2 at 90 secs.

The occurrence of maxima in weight gained vs time of immersion curve indicates the evidence of counter diffusion between zinc and mercury. Also the maxima revealed at different immersion time implies the importance of grain boundary diffusion.

(iii) Wetting Experiment with Single Crystal Specimen

Two groups of single crystals grown by different growth rate were used in this experiment. The clean and oxide free surface was obtained by electric polishing in the mixture solution of 25g Cr_2O_3, 7ccH_2O and 133cc conc. CH_3COOH with 18 volt. Then the crystals were coated in 50cc

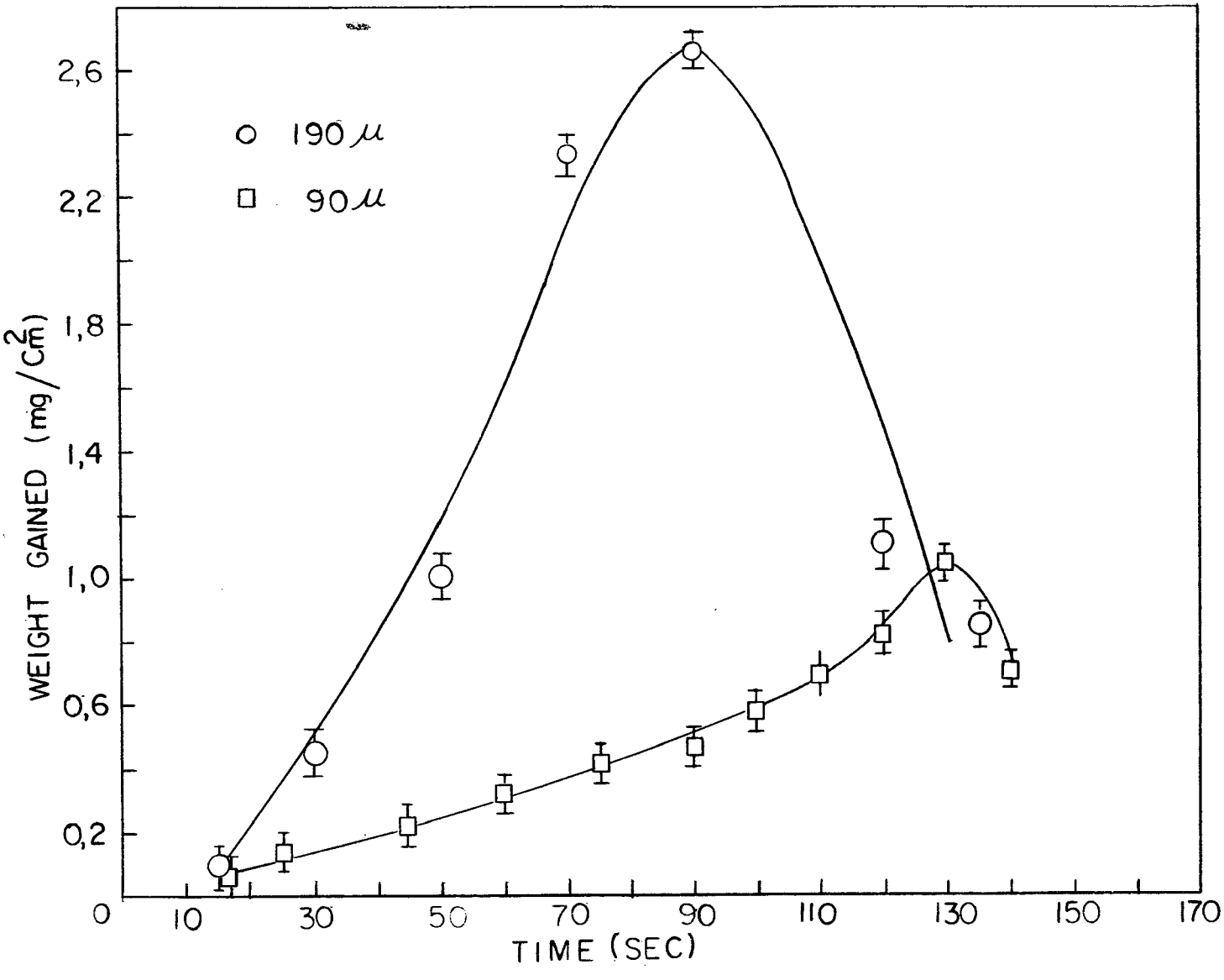

Fig. 4. Weight Gained per Unit Area of the Surface by Polycrystalline Specimens.

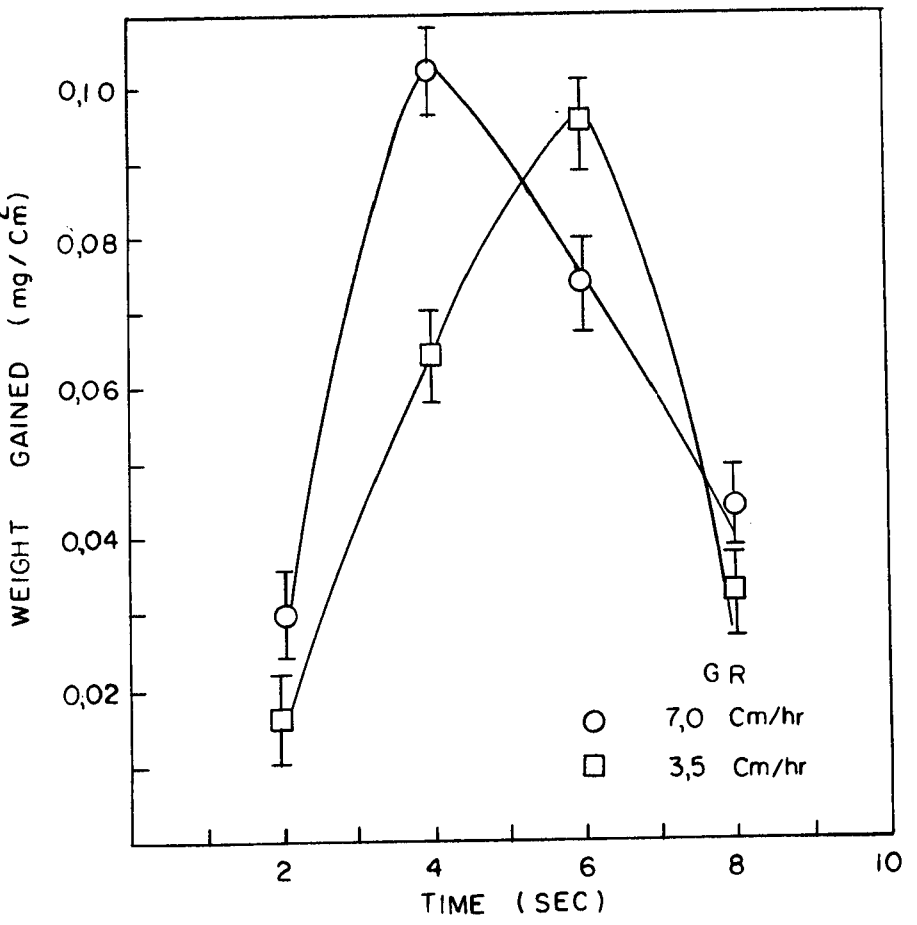

Fig. 5. Weight Gained per Unit Area of the Surface by Single Crystal Specimens.

clean mercury and the weight gained per unit surface area determined by the same technique used for polycrystalline specimens. The result is shown in Fig. 5.

As the case of polycrystalline specimens, weight gained per unit surface area vs time of immersion curves also revealed maxima. The idea of preparing two groups of monocrystals by the different growth rate was to detect the effect of density of structural defect (vacancy or dislocation) on wetting characteristics. The discrepancy of maxima between these two groups of crystals, however, appears to be due to the difference of surface condition (degree of micro relief) and not that of density of structural defects.

B. TENSILE TEST OF UNCOATED CRYSTALS

The shear stress-strain curve produced by the slip on h.c.p. metal is illustrated by the well known three stage in Fig. 6.

In order to investigate the effect of mercury coating on the deformation characteristics of zinc single crystals, the following parameters were defined and studied.

(1) The critical resolved shear stress τ_c, determined from the stress at which the shear stress-strain curve first deviates from linearity.

(2) The transition strain γ_{A-B}, from stage A to stage B determined by the strain at which the linear stage A ends.

(3) The work hardening slopes θ_A and θ_B which were measured from the slopes of the shear stress-strain curve in stage A and B.

(4) The fracture stress τ_f and strain γ_f at which the specimen failed.

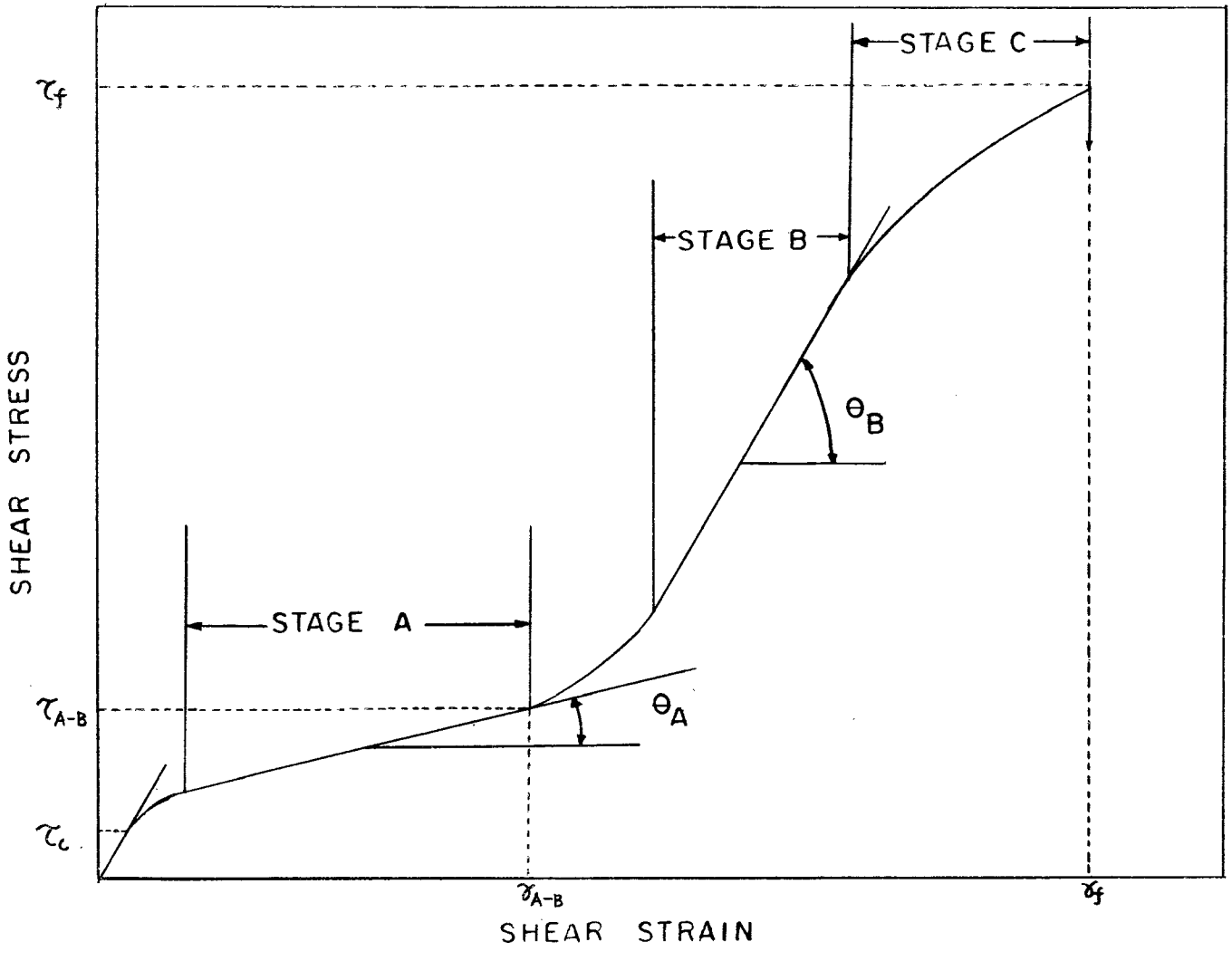

Fig. 6. The Three Stage Shear Stress-Strain Curve for h.c.p. Single Crystal.

Three uncoated specimens were tested ar room temperature to obtain standard values of above mentioned parameters and then compared with the results of subsequent experiments. The resolved shear stress-shear strain curves were obtained from the load-elongation chart using the formula given by Boas[18]. The relations are given by

$$\tau = \frac{P}{A} \sin X_o \quad \frac{l_o}{l} \left(\sqrt{\left(\frac{l}{l_o}\right)^2 - \sin^2 \lambda_o} \right) \qquad \ldots\ldots 5$$

and

$$\gamma = \frac{1}{\sin X_o} \left(\sqrt{\left(\frac{l}{l_o}\right)^2 - \sin^2 \lambda_o} - \cos \lambda_o \right) \qquad \ldots\ldots 6$$

where P is tensile load, A is original area of cross section, l_o is initial gauge length, l is gauge length after deformation, X_o and λ_o have the same meaning as defined before. Fig. 7 shows resolved shear stress-strain curves of uncoated crystals for the tensile test performed at room temperature with a strain rate of 0.1"/min. The results are summarized in Table II.

TABLE II

The values of parameters obtained by tensile test of uncoated crystals

Spec. No.	τ_c (Kg/cm^2)	θ_A (Kg/cm^2/u.s.)	γ_{A-B} (%)	τ_{A-B} (Kg/cm^2)	θ_B (Kg/cm^2/u.s.)	γ_f (%)	τ_f (Kg/cm^2)
ZXS-X-1	1.71	10.3	150	19	62.5	413	101
ZXS-C-3	1.69	11.2	140	20	63.0	394	103
ZXS-K-2	1.76	10.5	135	19	80.0	356	80

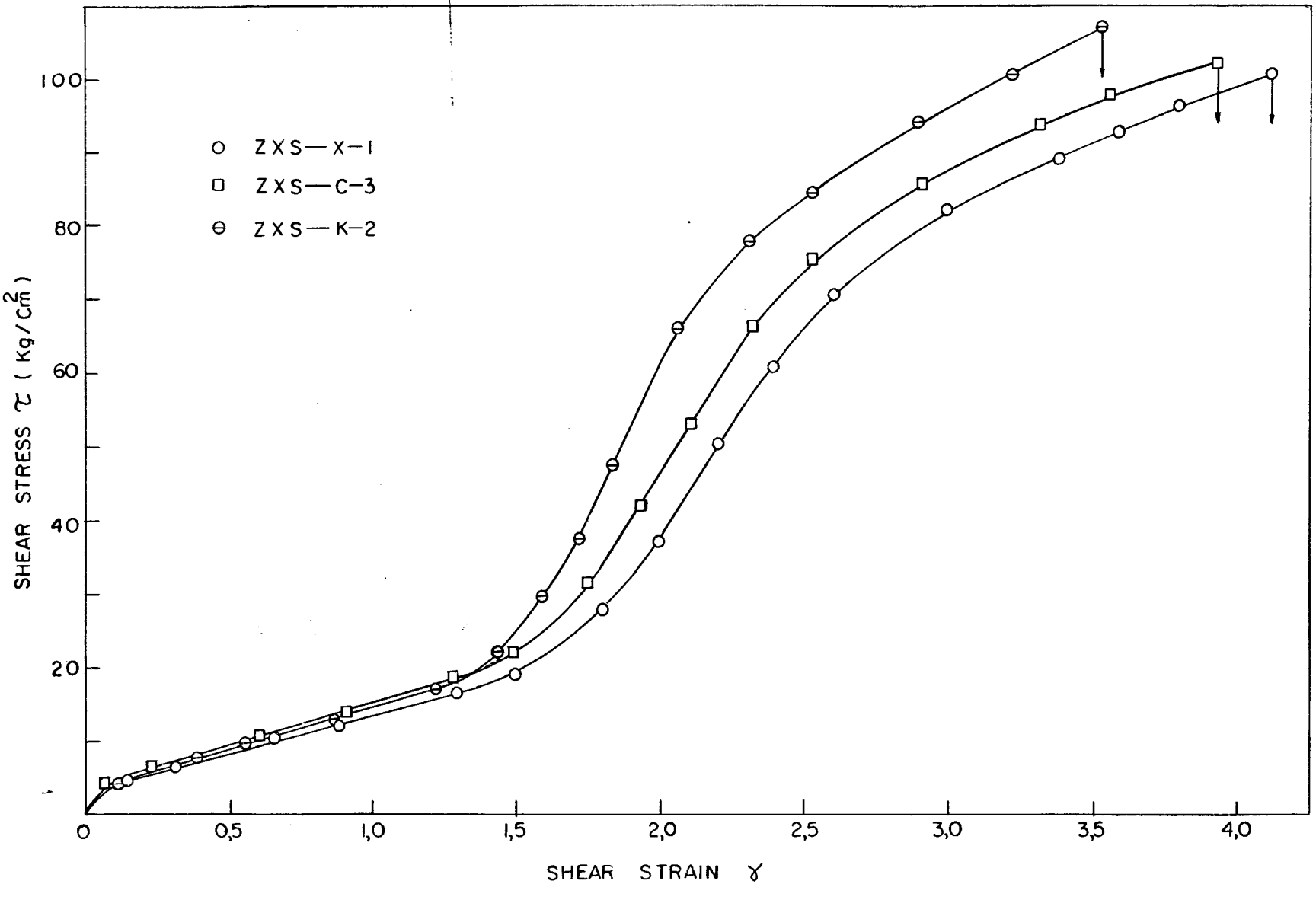

Fig. 7. Shear Stress-Strain Curves for Uncoated Crystals Tested in Tension at Room Temperature.

C. THE EFFECT OF TIME OF IMMERSION ON THE WORK HARDENING CHARACTERISTICS

A series of experiments were done to investigate the effect of immersion time on the work hardening characteristics under the premise that amount of mercury picked up by zinc monocrystals increases with immersion time. In this series of experiments, both ends of the crystal near grips were not protected and during the immersion, they were also coated by mercury. The amount of mercury used was 50cc. The exposure time between wetting and testing was fixed for 5 mins. Then, the coated specimens were tested at room temperature with a strain rate of 0.1"/min. More than half of the specimens failed at kink bands in the vicinity of grips. The mounting alloy (solder) exposed to mercury during coating adsorbed more mercury than central part of the crystal so that kinks formed near the grips were in more favourable condition for heavy mercury coating. Table III shows the testing results when time of immersion changed from 2 secs to 8 secs. Fracture stress and strain were not included in the table because unexpected early failure of specimens at grips revealed wide spreading results which have no value of comparison. The results can be summarized as follows.

(1) Critical resolved shear stress was increased by mercury coating and dependent on time of immersion.

(2) Work hardening slope in stage A was increased compared to the uncoated crystals, but the increase was almost insensitive to time of immersion.

(3) Transition strain from stage A to B had a decreasing tendency with time of immersion.

(4) The change of transition stress τ_{A-B} was quite random.

(5) Work hardening slope in stage B increased slightly but early failure of specimens with an immersion time beyond 8 secs made it obscure to prove.

TABLE III

The Effect of Immersion Time on the Work Hardening Characteristics

Specimen No.	τ_c(Kg/cm^2)	θ_A(Kg/cm^2/u.s.)	γ_{A-B}(%)	τ_{A-B}(Kg/cm^2)	θ_B(Kg/cm^2/u.s.)	Time of Immersion (secs)
ZXS-W-3	1.76	10.0	125	16	86	2
ZXS-H-2	1.25	12.2	125	23	70	2
ZNX-F-2	1.8	12.0	115	20	50	2
ZXS-J-1	1.77	10.0	115	16	75	4
ZXS-G-3	1.79	13.0	125	20	80	4
ZXII-E-1	1.81	8.5	125	13	60	4
ZXS-W-2	1.83	11.4	110	16	-	6
ZXS-G-1	1.84	11.8	115	19	-	6
ZXO-E-2	1.82	11.0	125	17	85	6
ZXS-U-1	1.96	12.3	100	15	-	8
ZXS-D-1	2.0	12.0	-	-	-	8
ZXII-B-2	2.03	-	-	-	-	8

D. THE EFFECT OF EXPOSURE TIME IN AIR AFTER MERCURY COATING ON THE WORK HARDENING CHARACTERISTICS.

Diffusion is a time dependent process. Therefore exposure of coated specimens in air for a certain time should intensify the effect of embrittlement if the embrittlement is due to the diffused surface active liquid metal into the crystals.

In this experiment, both ends of the specimen near grips were protected by wrapping them with polyethylene paper. At the same time, mounting alloy exposed at grips was covered by MICROSTOP to keep the alloy from mercury. Then, the specimens were coated with mercury by immersing them into 50cc clean mercury for 8 secs and tested at room temperature with a strain rate of 0.1"/min. Fig. 8-9 show the results when exposure time was increased gradually from 5 mins to 15 mins. The effect of exposure time in air after coating on the work hardening characteristics is given in Table IV.

The results can be summarized as follows:

(1) The mercury coating increased τ_c compared to that of uncoated specimens and the increase was dependent on time of exposure in air after coating.

(2) Work hardening slope in stage A was increased compared to uncoated crystals with decreasing tendency to a value similar to that of uncoated crystals as the time of exposure increases.

(3) Transition strain from stage A to B was remarkably decreased with time of exposure and the stage B was eliminated after 30 mins. exposure in air. Fig. 10 shows the reduction of fracture strain with the time of exposure in air.

(4) The transition stress τ_{A-B} was in the neighbourhood of that of uncoated specimen. However these values were generally higher than the corresponding stresses of the same amount of strain in uncoated specimens.

(5) Work hardening slope in stage B was also increased compared to uncoated crystals.

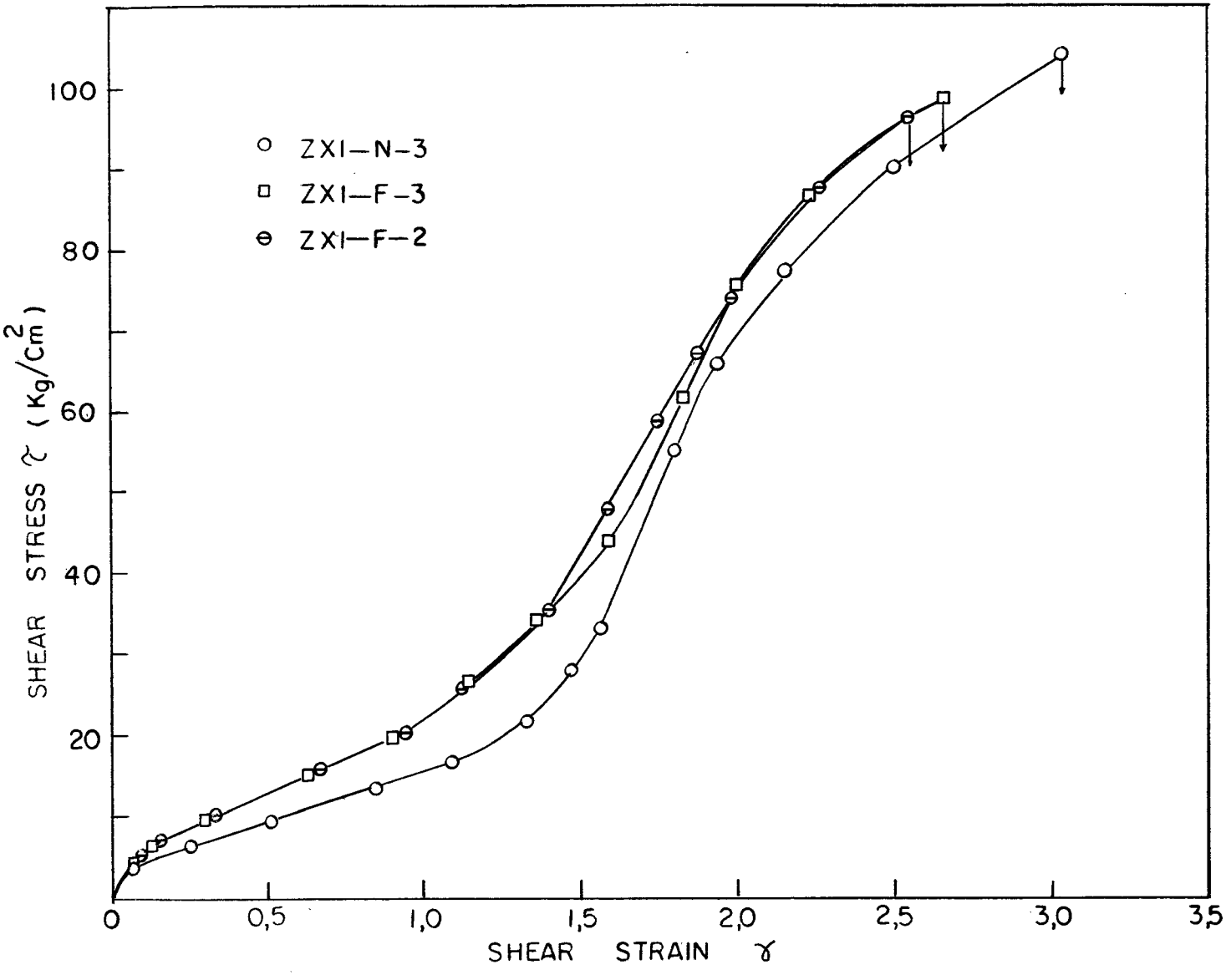

Fig. 8. Shear Stress-Strain Curves for Coated Crystals Tested in Tension at Room Temperature (Time of Exposure in Air after Coating: 5 mins)

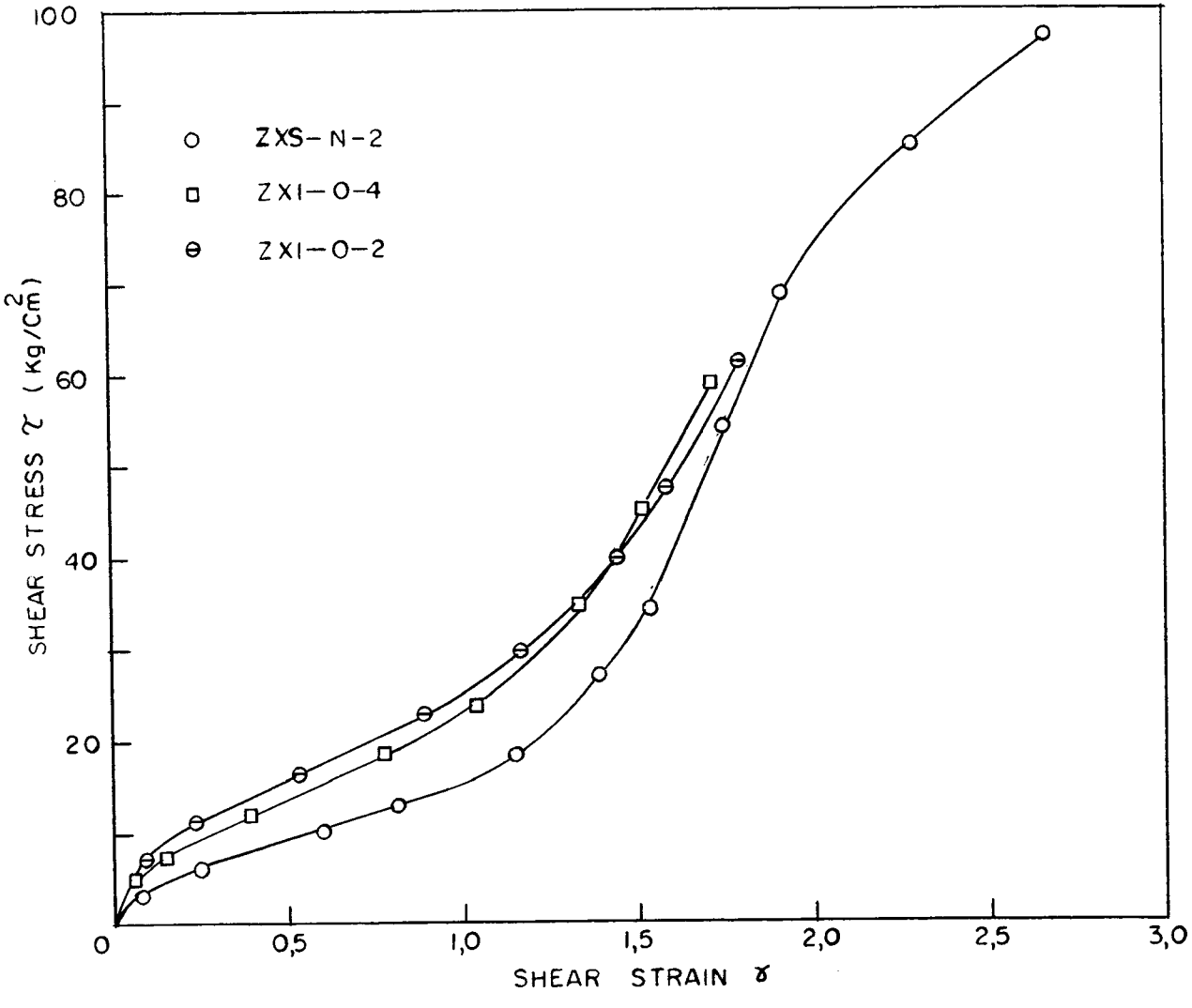

Fig. 9. Shear Stress-Strain Curves for Coated Crystals Tested in Tension at Room Temperature (Time of Exposure in Air after Coating: 10 and 15 mins.)

TABLE IV

The Effect of Exposure Time in Air after Mercury Coating on Work Hardening Characteristics

Specimen No.	τ_c (Kg/cm^2)	Θ_A (kg/cm^2/u.s.)	γ_{A-B} (%)	τ_{A-B} (Kg/cm^2)	Θ_B (Kg/cm^{2}u.s.)	τ_f (Kg/cm^2)	γ_f (%)	Time of Exposure (min)
ZXI-N-3	2.00	13.3	110	17	95	104.1	304	5
ZXS-F-3	1.99	17.2	95	21	75	100.0	254	5
ZXS-F-2	1.95	17.2	100	22	70	97.6	267	5
ZXS-N-2	2.03	12.0	100	16	95	97.0	267	10
ZXI-0-4	2.03	16.0	90	21	70	59.0	173	15
ZXI-0-2	2.06	17.1	80	21	65	61.6	179	15
ZXI-M-3	2.07	12.6	-	-	-	13.2	62	30
ZXI-M-2	2.12	14.3	-	-	-	14.5	72	30
ZXI-L-4	2.12	13.6	-	-	-	8.7	33	60
ZXI-0-3	2.11	9.7	-	-	-	6.1	38	60

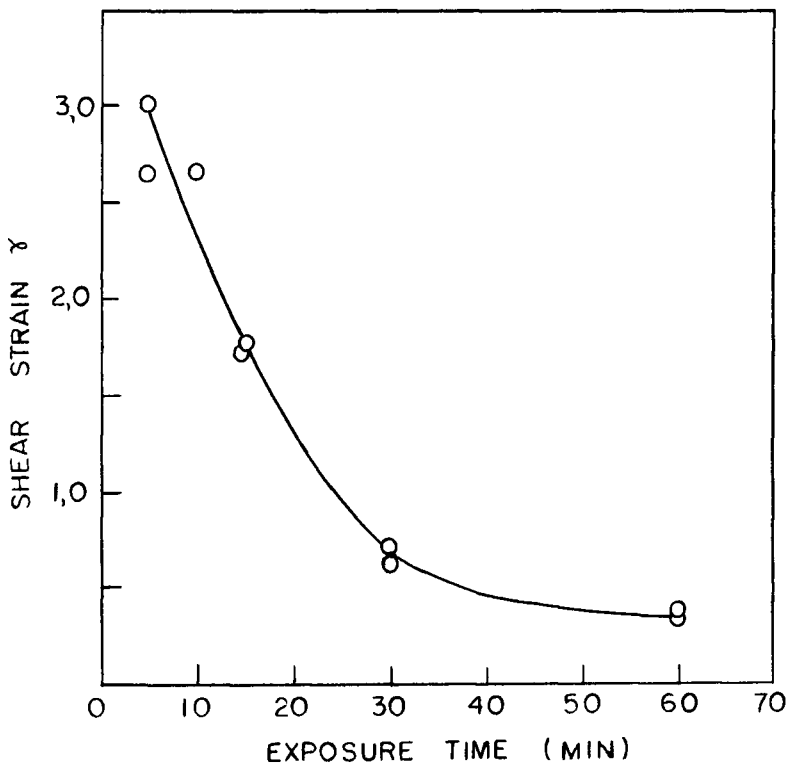

Fig. 10. The Effect of Exposure Time after Coating on Fracture Strain.

E. THE EFFECT OF PRESTRAIN AND MERCURY COATING ON THE WORK HARDENING CHARACTERISTICS.

The structural defects increase as deformation proceeds. If the interactions between structural defects and diffused surface active liquid metal causes the embrittlement, the amount of prestrain should modify the work hardening characteristics of zinc monocrystal coated with mercury.

After clean crystals were prestrained up to certain amount of shear strain, they were removed from INSTRON and both ends of crystals were protected

before mercury coating. Then those specimens with protected ends were immersed in 50cc mercury for 8 secs. Test was resumed after 10 min wrapping and subsequent 5mm exposure in air. Fig. 11-13 show the shear stress-strain curve with gradually increased amount of prestrain. The effect of prestrain and mercury coating on deformation parameters is given in Table V.

The results can be summarized as follows:

(1) Critical resolved shear stress, τ_c, work hardening slope in stage A, θ_A and transition strain γ_{A-B} were not affected since the tests were performed under the same conditions as those of uncoated crystals.

(2) Prestrain and mercury coating affected the amount of elongation markedly. If γ_{ps} stands for the amount of prestrain, the results show that $\gamma_f - \gamma_{ps}$ decreases with prestrain. The change of $\gamma_f - \gamma_{ps}$ was not significant up to 100% prestrain but after that dropped drastically. This relation is shown in Fig. 14.

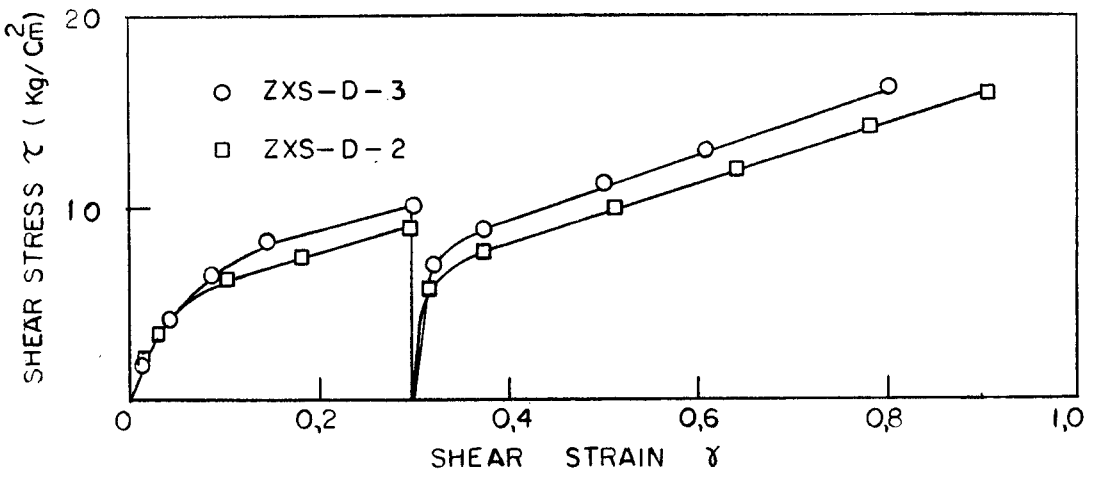

Fig. 11. Shear Stress-Strain Curves for Prestrained and Coated Crystals Tested in Tension at Room Temperature.

TABLE V.

The Effect of prestrain and Mercury Coating on Work Hardening Characteristics

Specimen No.	τ_c(Kg/cm^2)	θ_A(Kg/cm^2/u.s.)	γ_{A-B}(%)	τ_{A-B}(Kg/cm^2)	τ_f(Kg/cm^2)	γ_f(%)	Amount(%) of Prestrain
ZXS-D-3	1.81	10.0	-	-	16.2	81	30
ZXS-D-2	1.69	10.3	-	-	16.3	91	30
ZXI-P-2	1.67	11.0	-	-	19.2	151	100
ZXS-L-2	1.78	13.0	-	-	26.2	153	105
ZXI-P-4	1.63	10.0	125	17.5	40.8	184	162
ZXI-P-3	1.65	10.0	140	18.0	37.7	191	165

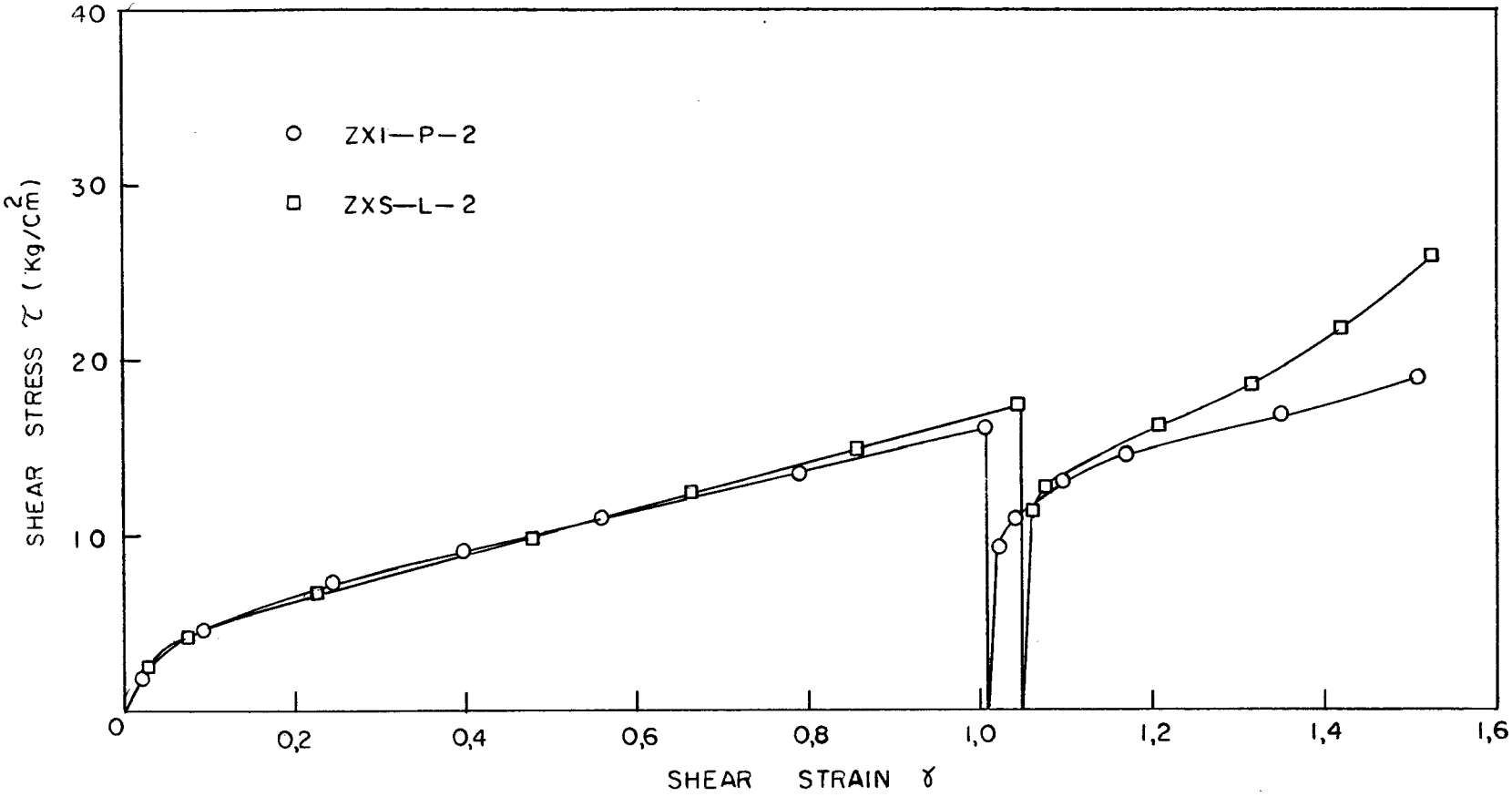

Fig. 12. Shear Stress-Strain Curves for Prestrained and Coated Crystals Tested in Tension at Room Temperature.

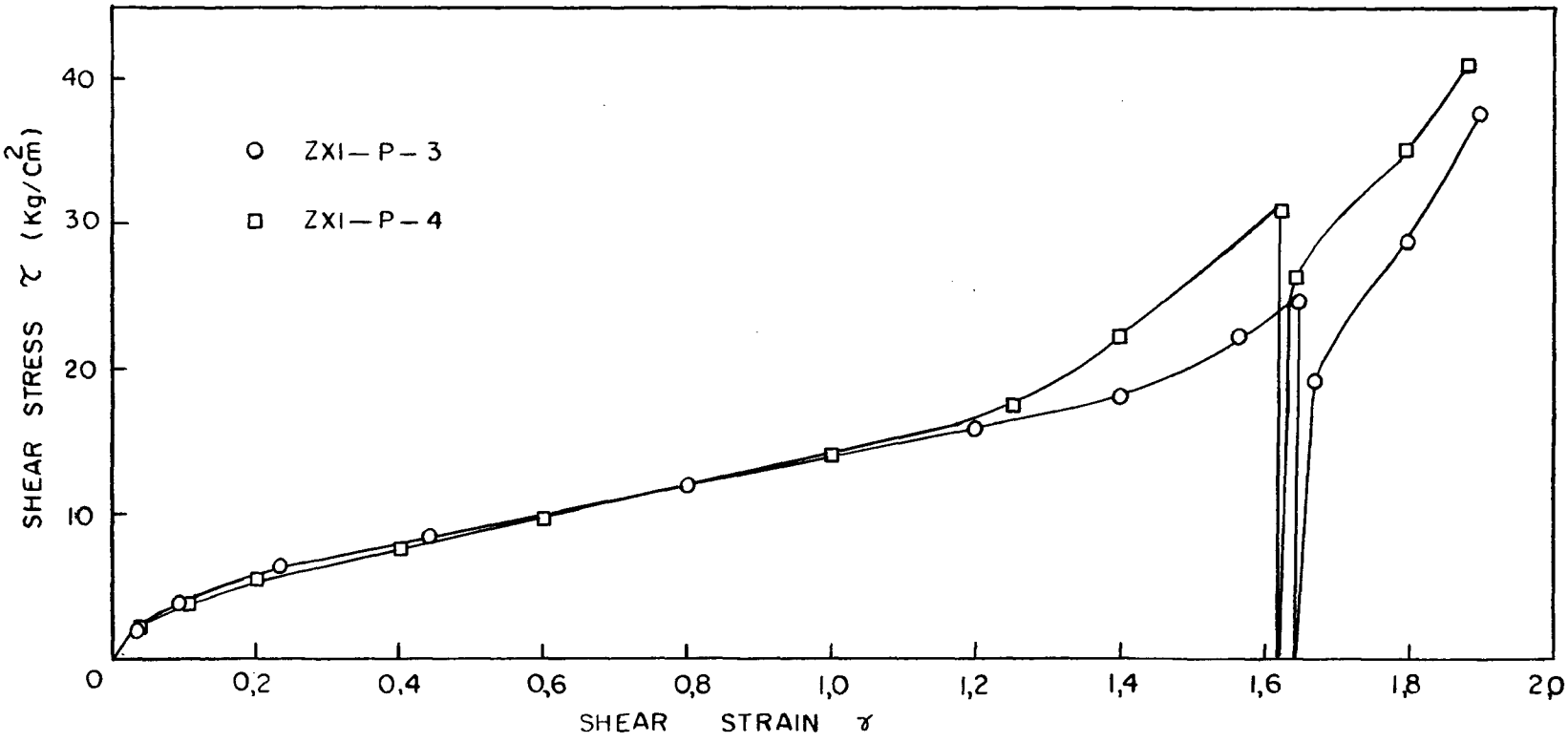

Fig. 13. Shear Stress-Strain Curves for Prestrained and Coated Crystals Tested in Tension at Room Temperatures.

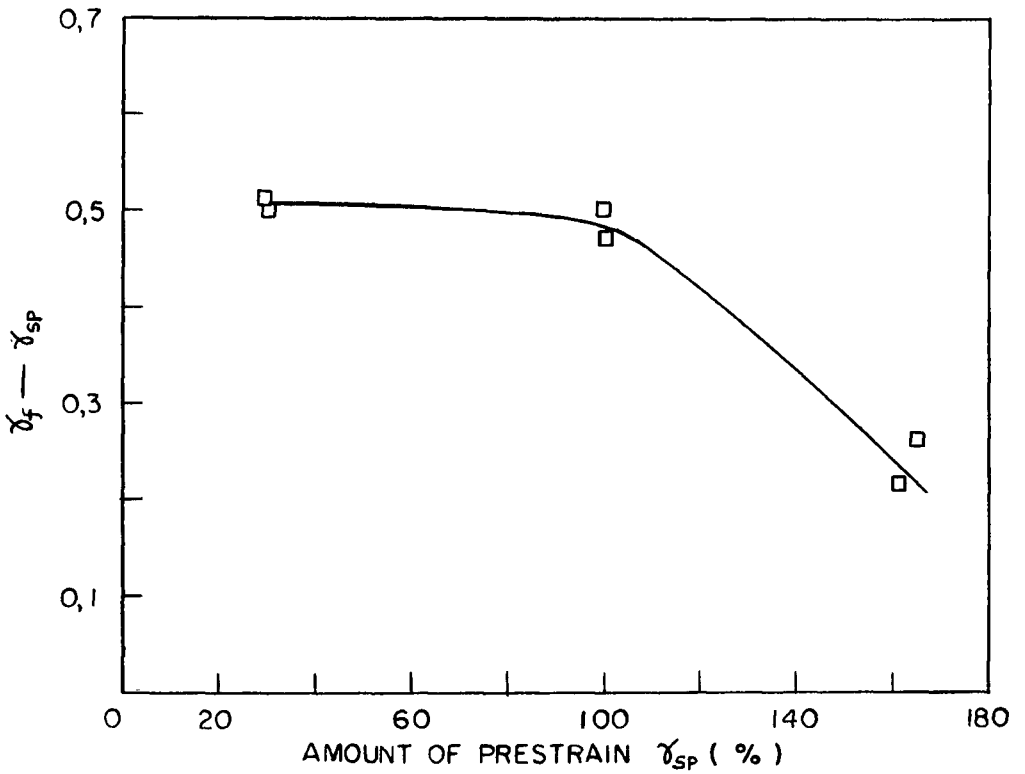

Fig. 14. The Effect of Prestrain and Mercury Coating on $\gamma_f - \gamma_{sp}$

F. THE EFFECT OF MERCURY COATING AND HIGH TEMPERATURE ON THE WORK HARDENING CHARACTERISTICS.

The importance of surface and lattice diffusion is evident from the experiments of exposure time and it has become valuable to establish the effect of higher temperature. Diffusion processes will be accelerated at higher temperature and more drastic embrittlement should be resulted.

In order to assess the effect of mercury coating and higher

temperature on the work hardening characteristics of zinc monocrystals, the following experimental procedures were involved. The specimens with protected ends were coated with mercury by immersing them into 50cc clean mercury for 8 secs. After 5 mins exposure in air, the coated specimen was brought to INSTRON and hot water bath was placed around the specimen. The water bath was heated by vertical type immersion heater by controlling the input power with a variac. The temperature was measured with mercury thermometer every three minutes. The temperature variation was negligible considering short time of testing resulting from early failure of specimens. ($T = t° \pm 1°$). Coated specimens were held at desired high temperature for 5 mins and then hot water bath was replaced by cold water bath to cool the specimens down to room temperature again. Then the specimens were pulled by INSTRON with a strain rate of 0.1"/min. The effect of mercury coating and higher temperature on the work hardening characteristics is given in Table VI.

TABLE VI

The Effect of Mercury Coating and Preheating on Room Temperature Deformation Characteristics

Specimen No.	τ_c (Kg/cm^2)	θ_A (Kg/cm^2/u.s.)	γ_{A-B} (%)	θ_B (Kg/cm^2/u.s.)	τ_f (Kg/cm^2)	γ_f (%)	Preheat Temp. °C
ZXI-V-2	2.09	12.0	-	-	13.4	85.7	50
ZXI-V-3	2.20	11.0	-	-	13.2	89.7	50
ZXI-W-3	2.30	15.7	-	-	7.5	30.0	75
ZXI-V-1	2.24	13.8	-	-	9.3	44.0	75
ZXI-Y-3	2.52	-	-	-	4.6	6.7	95
ZXI-Y-2	2.46	-	-	-	5.5	9.8	95

The results can be summarized as follows:

(1) The stage B was completely eliminated in these experiments indicating severe embrittlement effect. Critical shear stress τ_c was increased as the temperature increased.

(2) The fracture stress and strain were decreased with the temperature. Fig. 15 shows the effect of mercury coating and high temperature on fracture strain.

(3) There was a tendency such that θ_A increases as the heating temperature increased. However, the earlier failures resulting from 5 min. holding at 95°C eliminated the sufficient appearance of stage A making assessment of the result difficult.

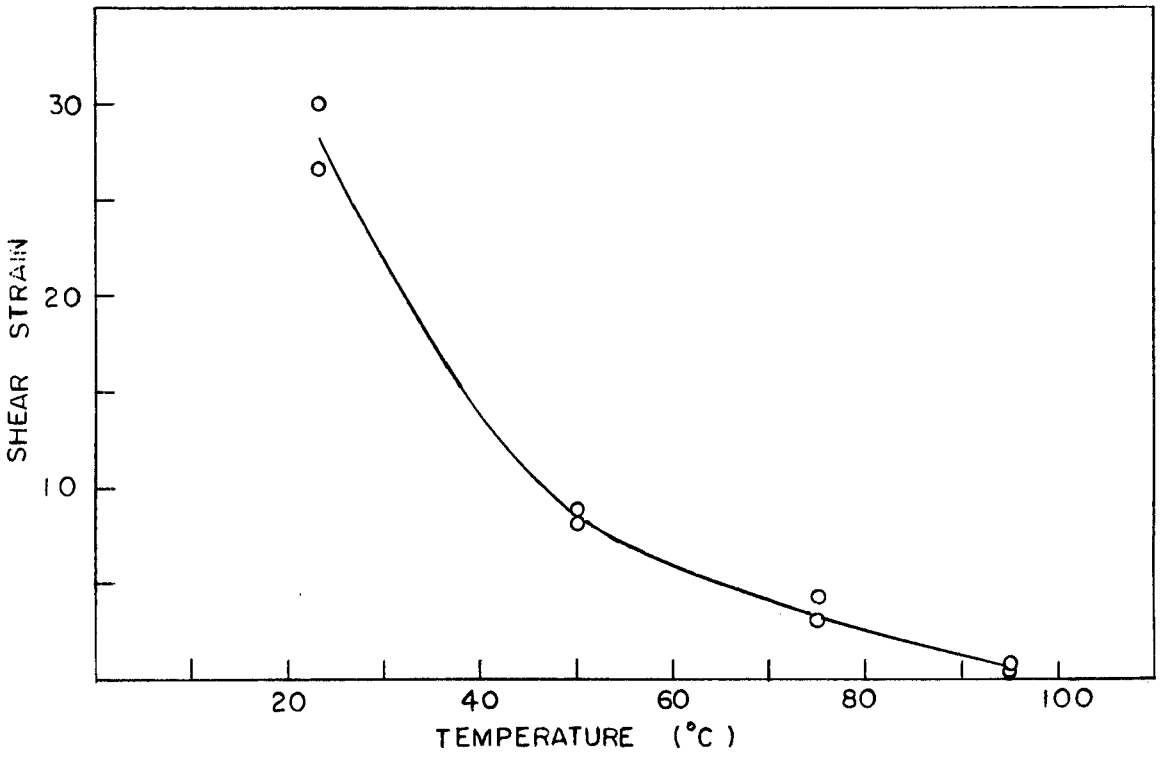

Fig. 15. The Effect of Mercury Coating and Higher Temperatures on Fracture Strain.

G. SUMMARY OF RESULTS

(1) The weight gained vs immersion time curves obtained from mercury coating experiments show maxima in both polycrystalline and monocrystal specimens. This implies the evidence of high counter diffusion between zinc and mercury when they are in contact with each other.

(2) In non-coated crystals, the critical resolved shear stress is $1.72 Kg/cm^2$ and $\frac{\Theta_A}{G} = 3.05 \times 10^{-5}$ is observed for the crystal orientation of $X_o = 46 \pm 3°$ and $\lambda_o = 46 \pm 4°$. The relation between Θ_A and Θ_B is $\Theta_B = 6\Theta_A$. ($\tau_c = 1.8 Kg/cm^2$ by Jillson[19]).

(3) The mercury coating increases critical resolved shear stress ($\tau_c = 1.99 Kg/cm^2$ for 8 secs immersion and 5 mins exposure time in air) and the increase is dependent of exposure time in air after coating.

(4) The work hardening slopes (Θ_A and Θ_B) are increased by mercury coating and exposure in air before testing. Under the same experimental conditions, transition strain γ_{A-B} is decreased remarkably and the stage B is eliminated after 30 mins exposure in air. Also fracture stress and strain are decreased with exposure time in air.

(5) The prestrain and mercury coating cause the earlier failure of crystals. The reduction of $\gamma_f - \gamma_{sp}$ (γ_{sp} = amount of prestrain) is not significant up to 100% prestrain and after that drops drastically.

(6) When coated crystals are treated at elevated temperatures, increased critical resolved shear stress is observed. Also high temperature treatment eliminates stage B, and the fracture stress and strain are reduced as the heating temperature increases.

H. REPRODUCIBILITY OF RESULTS

Typical of experiments with single crystals, the present results showed a scatter of ± 15% in most of the measured parameters. Accordingly, a minimum of two specimens were tested under given experimental conditions, and the results quoted for each condition are the arithmetic mean of all tests.

IV. METALLOGRAPHIC OBSERVATIONS

An attempt has been made to observe the slip markings of mercury coated crystals which were deformed under various experimental conditions.

Fig. 16 shows the slip lines of an uncoated crystal deformed at room temperature. Wide deformation twin bands are observed. The wavy characteristics of slip lines are the evidence of dynamic recovery during the deformation resulting from the climb of edge dislocations.

Small humps, which are tensile kink "embryos", are observed as at A in Fig. 16. The causes of these humps may be either the stress concentration on pits and trapped oxide or non-uniform distribution of tensile stress across slip planes.

Fig. 17-21 show the surface of deformed crystals coated with mercury when time of exposure in air after coating increases from 5 mins. to 60 mins. At the beginning, the size and number of embryos increases with exposure time until the time reaches 15 mins. After that we observe fewer and smaller embryos on the surface of deformed crystals. This behaviour is understandable since tensile kink embryos should occur after substantial strain, and the reduced ductility that results from long exposure to mercury limits their formation.

Fig. 22-23 show the deformation markings of coated crystals tested at room temperature after they were treated at elevated temperature (50°C and 75°C). We observe well developed embryos on the surface of the crystal which was treated at the lower temperature. This crystal has a fair amount of ductility. However,

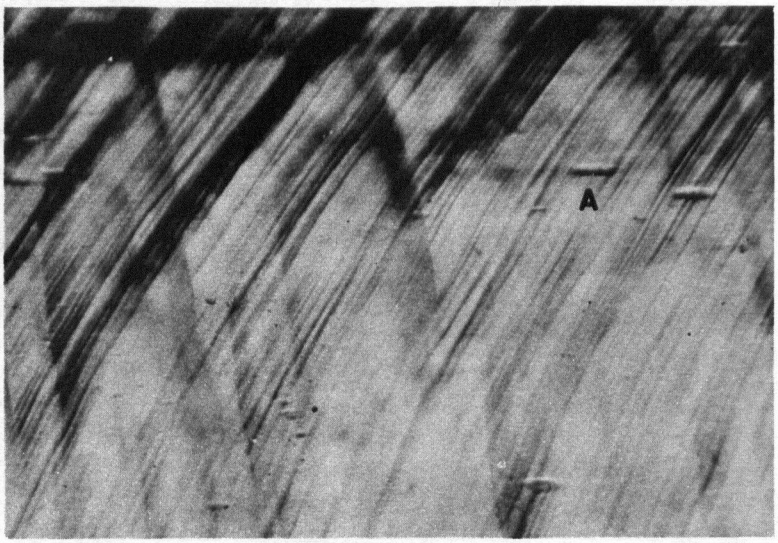

Fig. 16. ZXI-I-3 x 230
(Uncoated and Tested at Room Temperature).

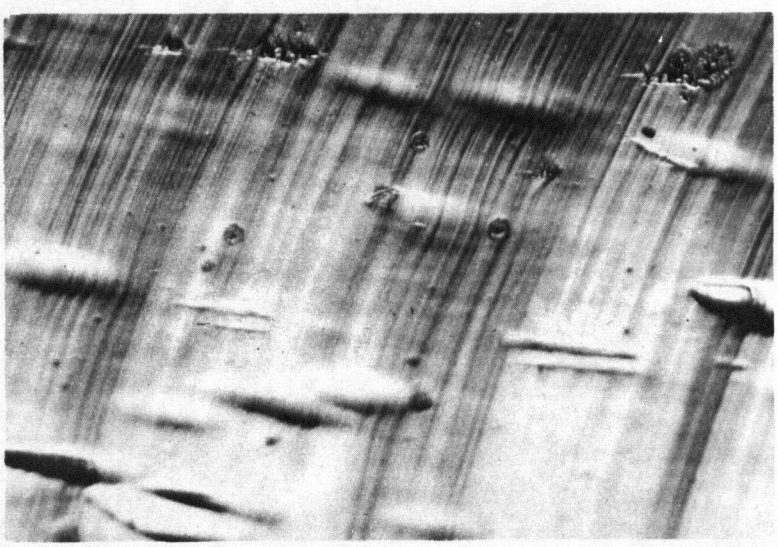

Fig. 17. ZXI-N-3 x 230
(Coated and Tested at Room Temperature.
Time of Exposure in Air: 5 mins.)

Fig. 18. ZXI-N-2 x 230
(Coated and Tested at Room Temperature.
Time of Exposure in Air: 10 mins.)

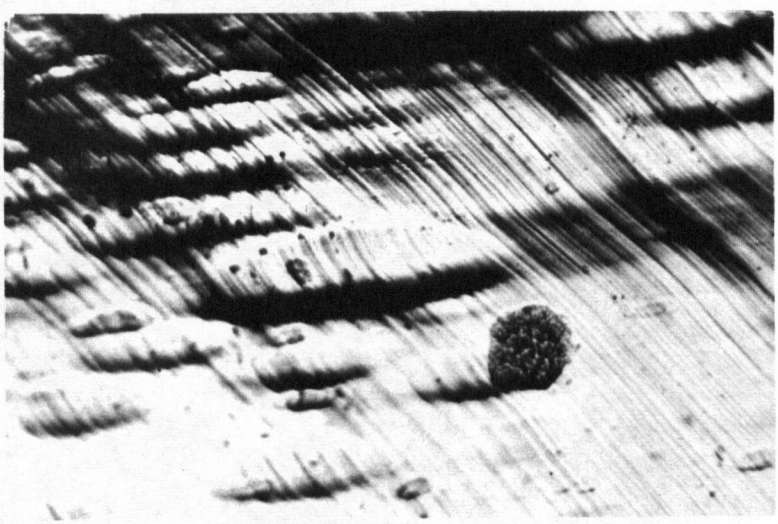

Fig. 19. ZXI-0-4 x 230
(Coated and Tested at Room Temperature.
Time of Exposure in Air: 15 mins.)

Fig. 20. ZXI-M-2 x 230
(Coated and Tested at Room Temperature.
Time of Exposure in Air: 30 mins.)

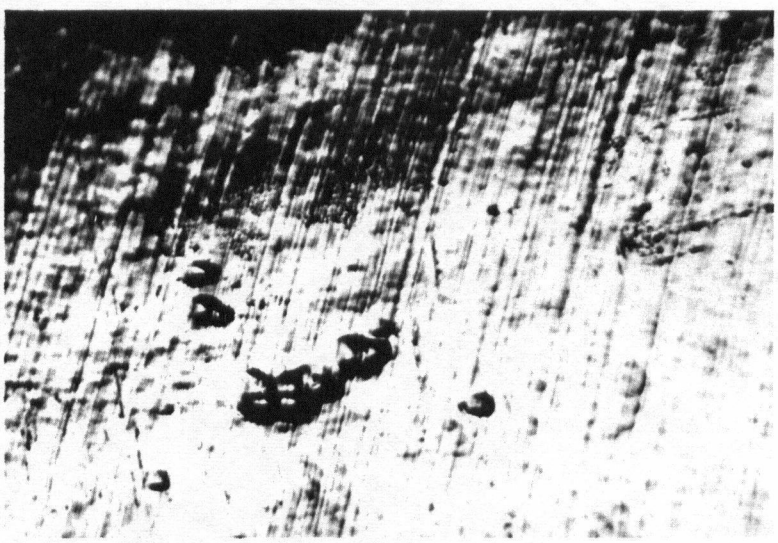

Fig. 21. ZXI-0-3 x230
(Coated and Tested at Room Temperature.
Time of Exposure in Air: 60 mins.)

Fig. 22. ZXI-V-2 x 230
(Coated, 5 min. Exposure in Air, 5 min. in 50°C Bath and Quench to Room Temperature. Room Temperature Test.)

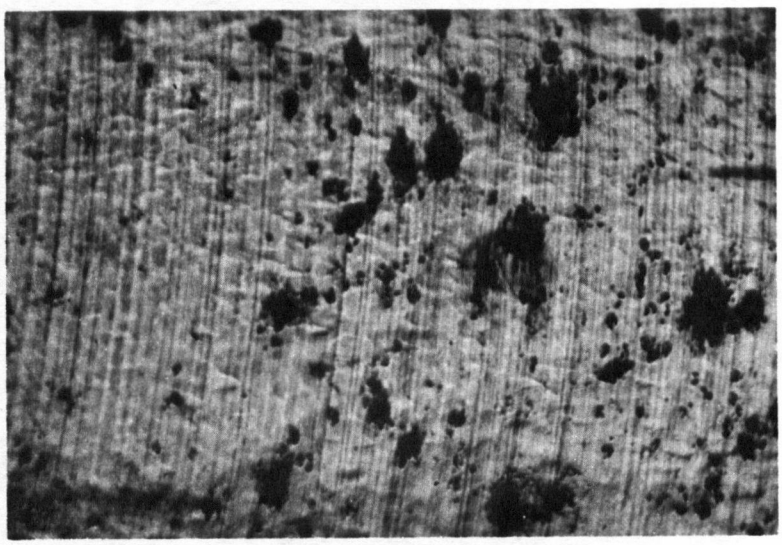

Fig. 23. ZXI-V-1 x 230
(Coated, 5 min. Exposure in Air, 5 min. in 75°C Bath and Quench to Room Temperature. Room Temperature Test.)

the reduction of ductility due to the higher temperature treatment eliminates the formation of embryos compared to lower temperature treated one.

Fracture surfaces were also carefully examined under the microscope to detect any evidences of crack initiation and propagation. Fig. 24 shows the initiation and propagation of crack developed in the uncoated crystal. A crack was initiated on (0001) matrix and propagated along (0001) twin. Fig. 25-27 show cracks for coated crystals which were initiated at kink bands and propagated along basal plane. Relevant mechanisms will be considered in the discussion part.

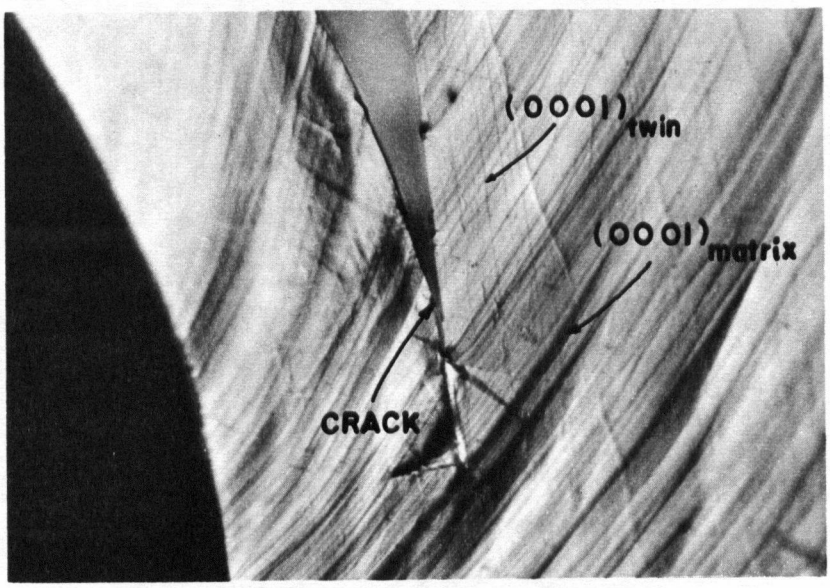

Fig. 24. Crack Initiated by Coalescence of Dislocations on Matrix Basal Plane Propagates along Basal Plane in Twin x 230.

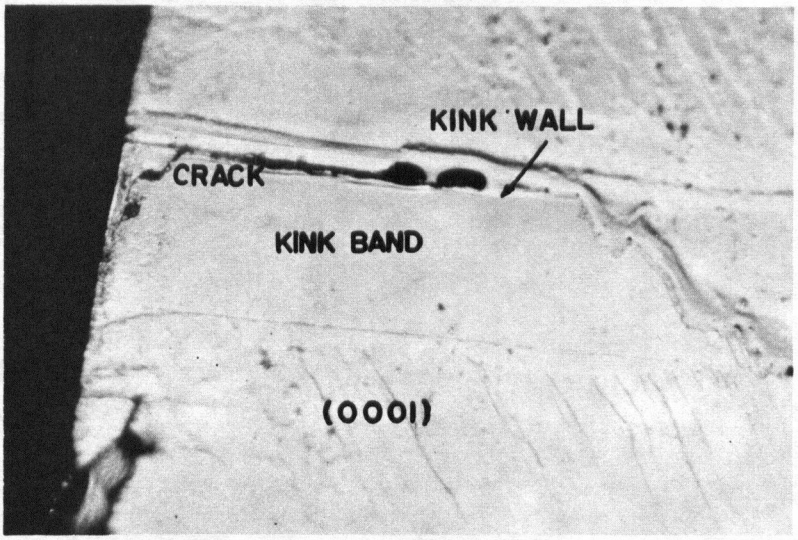

Fig. 25. Crack Initiated at Kink Wall x 230

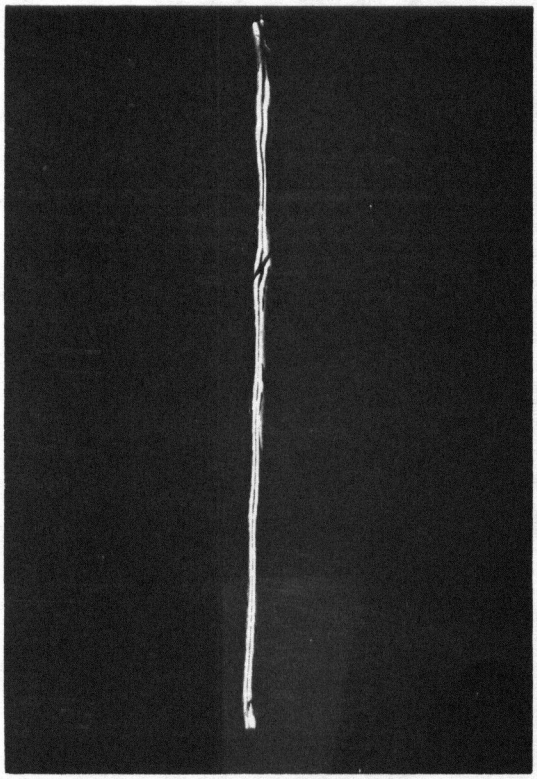

Fig. 26. Crack Initiated at Tensile Kink.

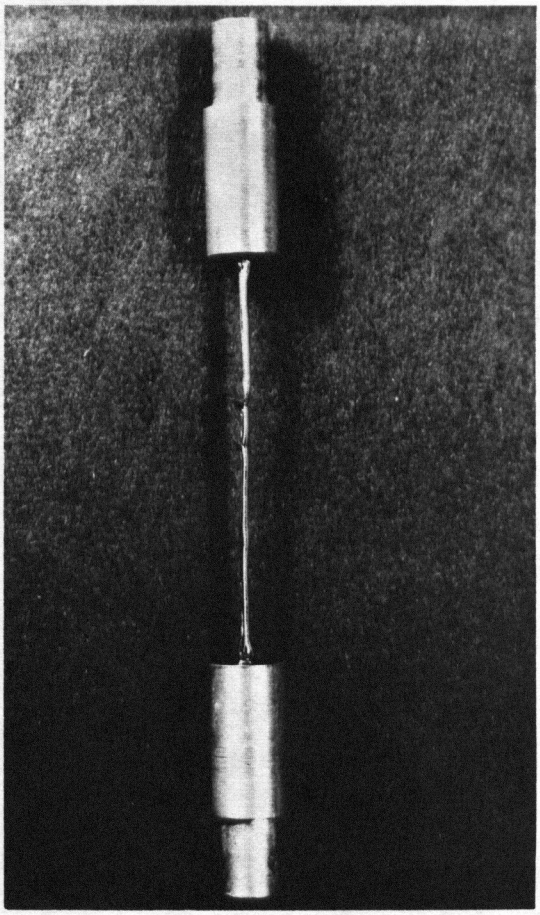

Fig. 27. Cracks Initiated at Tensile Kinks.

V. DISCUSSION

A. WETTING CHARACTERISTICS AND DIFFUSION OF MERCURY IN ZINC

Since the reduction of the mechanical strength and plasticity of zinc monocrystals results from mercury coating, it has become necessary to pay attention to the role played by wetting and diffusion.

(i) Wetting Characteristics

As a primary guide from the thermodynamics of the wetting of solid surfaces by liquid, we derive that a necessary condition for spreading is

$$\gamma_S > \gamma_L \qquad \ldots\ldots 7$$

where γ_S is the surface energy of solid and γ_L is that of liquid (see Appendix I). There is sizeable difference of surface energy between mercury and zinc (476 ergs/cm^2 for Hg[20] and 859 ergs/cm^2 for zinc[21]), which satisfies the condition of wetting.

(ii) The Diffusion of Mercury in Zinc

The weight gained vs time of immersion curve for polycrystalline specimens, when they are immersed into fixed amount of mercury, is quite different from that of monocrystals. This implies that structural defects play important roles in diffusion. The weight gained vs time of immersion curves for both polycrystalline and monocrystal specimen have revealed maxima indicating evident counter diffusion between mercury and zinc. At first the weight gained increased as the time of immersion up to the maximum point. During this period, the weight gained is larger than the loss of zinc resulting from counterdiffusion into mercury. After the maximum, the loss of zinc into the mercury predominates over the weight gained. Considering the density difference between mercury and

zinc, the occurrence of maxima in wetting experiments proves the fact that the diffusion of zinc into mercury appears to be very fast.

The wetting experiments with single crystals have also revealed maxima. However, the maxima occurred at earlier times of immersion than that of polycrystalline specimen.

Various attempts designed to explain the differences in weight gained and maxima times were not successful because of the complicated variables involved (grain boundary, concentration of structural defects and degree of micro relief etc.).

During the tensile deformation, microscopic surface steps will appear on the surface of crystal due to the slip revealing new surface of basal planes. Mercury coated over the surface of crystals will migrate on the newly exposed basal plane steps to reduce the overall surface energy (see Fig. 28).

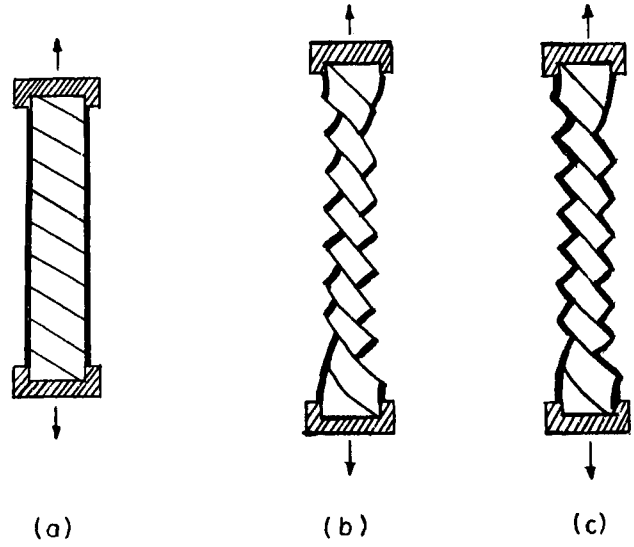

Fig. 28. Mercury Migration to Newly Exposed Basal Plane During Deformation. (a) Uniform Coating before Test (b) Exposure of New Basal Plane Free from Mercury (c) Mercury Migration to Newly Exposed Basal Plane by Surface Diffusion.

This migration is achieved by surface diffusion. Pleteneva and Fedoseeva[22] determined the coefficient of surface diffusion of mercury on zinc by measuring the rate of moving front of mercury on the surface of vertically clamped zinc specimen. This measurement satisfied a diffusional relation in which the height of mercury rise was directly proportional to the square root of the time. The determined value is 2.48×10^{2} cm^2/sec at 20°C which is much faster than the coefficient of bulk diffusion in zinc ($0.2.3 \times 10^{-11}$ cm^2/sec at 20°C).

In lattice diffusion, structural defects, (dislocation and sub-boundary) play important role. Love[23] has proposed an adequate model for dislocation pipe diffusion in which diffusion occurs along the line of vacant sites lying adjacent to the edge of extra inserted plane in an edge dislocation (see Appendix II). Therefore mercury atoms coated over the surface will diffuse through dislocation pipes. As the deformation proceeds more structural defects can be evolved and enhanced dislocation pipe diffusion is expected.

B. THE EFFECT OF MERCURY COATING ON THE CRITICAL RESOLVED SHEAR STRESS OF ZINC SINGLE CRYSTAL

In considering the cause of increased critical resolved shear stress of amalgamated crystals, the following three effects are relevant subjects to be discussed.

(i) Dislocation egress effect

(ii) Surface drag effect

(iii) Surface anchoring effect

According to the following arguments, the first two effects can not account for the cause of increased critical resolved shear stress.

(i) Dislocation Egress Effect

A barrier resulting from the change of surface condition would be expected to have an effect on the motion of dislocations and we shall call this effect the "dislocation egress effect". The image force tending to pull an edge dislocation out of the surface is resisted by the work done accompanying the formation of new surface area. This effect has been considered by Frank[24] when surfaces are clean. He came to the conclusion that, except for lead, most metallic crystal surfaces should offer no resistance to the egress of dislocations under their own image force. This idea was established by the fact that the energy of a dislocation located near the surface is always greater than would be associated with the newly exposed surface caused by egress of the dislocation. In the case of zinc, the surface resisting force, γb is 1.98×10^{-5} erg/cm (γ = surface energy and b= Burger's vector) and the energy of a dislocation a few atoms away from the surface is 2.63×10^{-5}erg/cm. In fact, the surface energy of a zinc crystal was reduced by the mercury coating making it easier for dislocations to egress out of the surface. Therefore, mercury coatings should have reduced the critical resolved shear stress if we consider the dislocation egress effect only.

(ii) Surface Drag Effect

Any resistance to the formation of new surface or shear at the surface would be expected to have an effect to the passage of the dislocations. This effect will be termed the "surface drag effect". Consider the possible effect

of such a surface drag on the operation of a Fisher single-ended surface source as shown in Fig. 29.

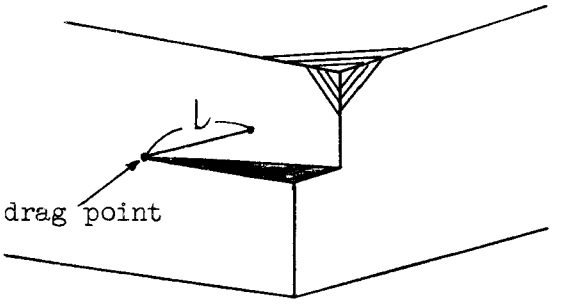

Fig. 29. Fisher Single-Ended Source.

At the critical stress τ_c to operate a single-ended source of length l, the force acting at the drag point is given by

$$\frac{\tau_c bl}{2} = \frac{Gb^2}{4} \qquad \ldots\ldots 8$$

where G is shear modulus and b is Burger's vector. The surface drag force is equal to γb where γ is the surface free energy of the crystal. The ratio, q, of the force acting at the drag point to the surface free energy is given by

$$q = \frac{Gb}{4\gamma} \qquad \ldots\ldots 9$$

Thus, when q is less than unity, the surface drag force exceeds the initial force to operate the surface source and dislocations will be pinned unless the stress is raised sufficiently. For the case of zinc q = 2.25 greater than unity. When the surface is clean, mercury coating reduces the surface energy further.

Therefore, we do not expect any surface drag effect from amalgamation of zinc monocrystals.

(iii) Surface Anchoring Effect

Dislocations that intersect the surface can be anchored as a consequence of selective lattice diffusion of surface active atom along the dislocation pipe. There is the additional possibility that dislocations located near to but not intersecting the surface may also be pinned by selective solute atmosphere or precipitate formation. This effect will be called "surface anchoring effect". Considering crystal structure of zinc and atomic size of zinc and mercury (Zn: 1.38Å and Hg = 1.57Å), which favours substitutional type of solution, possible interaction between dislocation and diffused mercury will be Suzuki type rather than Cottrell type. H. Suzuki has pointed out that partial dislocations with a stacking fault in between can interact with impurity atoms with a chemical form of interaction. The few atomic layers which constitute the stacking fault show f.c.c. structure (in f.c.c. stacking fault layers are C.P. Hex.) instead of hexagonal. Therefore the solid solubility of impurities contained in the matrix can very well differ "within" the stacking fault and "outside". The difference is a thermochemical nature and may contribute to an effective energy of binding of the impurity atoms to the extended dislocation. Once an extended dislocation aquires its equilibrium amount of solute it may be difficult to move compared to the free dislocation.

In view of foregoing argument, surface anchoring effect originated from selective lattice diffusion of mercury atom along the dislocation pipe or Suzuki type locking of dislocations surpasses the other two effects showing an

effect on increased critical resolved shear stress. Long exposure time after mercury coating and short time holding of coated crystals at elevated temperatures confirm the anchoring effect of diffused mercury atoms increasing the critical resolved shear stress.

C. THE EFFECT OF MERCURY COATING ON THE WORK HARDENING OF ZINC SINGLE CRYSTAL

The mercury coating on the surface of zinc single crystal has brought remarkable changes in the deformation characteristics such that crystals were embrittled with the following observed results.

(1) Increased work hardening slope in stage A.

(2) Decreased transition strain, γ_{A-B} from stage A to stage B.

(3) Increased work hardening slope in stage B.

(4) Decreased fracture stress and strain.

In the deformation of zinc single crystals, recovery processes are operative above -30°C. Mott[25] has proposed that static recovery is due to the climb motion of edge dislocations and suggested that dynamic recovery also could be based on the same atomic process. Seeger and Träuble[26] observed the fanning of slip lines, shown schematically in Fig. 30, which does not appear at lower temperature and came to the conclusion that the thermally activated recovery process in zinc is due to the climb motion of edge dislocations. This idea makes an attractive contrast in relationship to the case of face centered cubic metals in which cross slip by screw dislocations plays an analogous role for dynamic recovery.

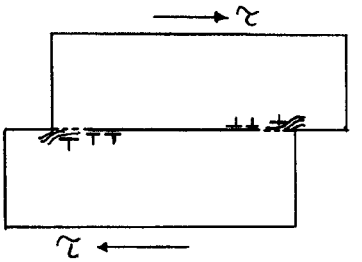

Fig. 30. Schematic Picture of Fanning Process at both ends of the same slip line.

Hirsch et al[27] have shown that highly mobile vacancies condense to form a dislocation ring. According to their argument, the anisotropic nature of the hexagonal crystal structure forces these dislocation rings to stay on the basal plane and they are highly immobile because their Burger's vector is perpendicular to the basal plane. Consequently, this kind of vacancy or vacancy group condensation which occurs in static or dynamic recovery process enables us to explain the observed work hardening characteristics of hexagonal metals. Dislocation rings with diameter less than 100Å have no substantial elastic stress field because of their dipole characteristics[26]. However, these dislocation rings can act as short range obstacles restraining the motion of glide dislocations. The number of vacancies is proportional to the degree of deformation and as a consequence, the number of dislocation rings also increases with strain. The unbalance of counter compensating processes, namely, the formation of dislocation rings and their elimination through the climb motion provide the understanding of work hardening in hexagonal metals. Though the dislocation rings are energetically more stable than atomically dispersed vacancies, they are not under thermodynamic equibrium. Therefore they can be annealed out by static or dynamic recovery process. The transition from stage A to B is attributed to a critical

concentration of dislocation rings resulting from the unbalance of the above mentioned counter compensating processes. The changes of work hardening characteristics of coated crystals can be explained by the interaction between dislocation rings and diffused mercury atom.

Microscopic examination to detect the distance of diffusion was not successful due to the lack of a distinct boundary resulting from the formation of any new phase or compound. Diffusion also occurs during the deformation and increased number of structural defects accelerate the diffusion process. The increased penetration of mercury atoms resulting from long exposure time or higher temperature treatment should cause more embrittlement, due to enhanced diffusion of mercury atoms and hence an increased interaction with the dislocation rings. Therefore a reduction of dynamic recovery results from the formation of stable short range obstacles, causing substantial changes in the work hardening characteristics.

From the arguments developed with the aid of deformation theory of hexagonal metals, we reach the following summaries.

(1) The interaction between diffused mercury atoms and dislocation rings is responsible for increased work hardening slope in stage A and decreased transition strain from stage A to B.

(2) Increased amount of prestrain introduces more dislocation rings which can interact with diffused mercury atoms resulting in early failure of crystals.

(3) High temperature tests support the role of diffusion in liquid metal embrittlement. High temperatures accelerate both surface and lattice diffusion promoting the possibilities of interaction between diffused

mercury atoms and dislocation rings.

(4) The increase of work hardening slope in stage B and decreased fracture stress and strain can be explained by analogous argument as already mentioned.

D. PROPOSED MECHANISM FOR CRACK INITIATION

In non-coated crystals tested in tension at room temperature, severe twinning preceded the fracture. Careful metallographic examination revealed that crack was propagated along the basal plane in twinned part. The relationship between the shear and the undistorted plane which describes the twinning in zinc can be illustrated by Fig. 31.

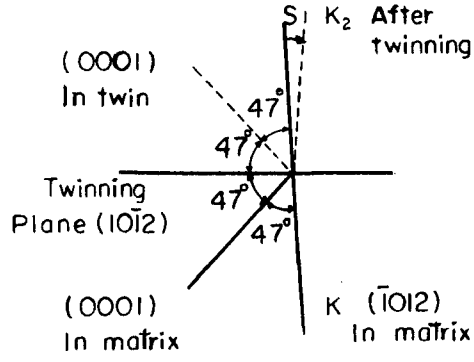

Fig. 31. Geometry of Twin in Zinc.

The common form of twin in zinc is a compound twin in which we have

$$K_1 = (10\bar{1}2) \qquad K_2 = (\bar{1}012)$$

$$\eta_1 = [\bar{1}011] \qquad \eta_2 = [10\bar{1}1]$$

where K_1 = the twinning plane or the first undistorted plane, K_2 = the second undistorted plane η_1 = shear direction and η_2 = the direction defined by the intersection of the plane of shear with K_2. The plane of shear is the plane which is mutually perpendicular to K_1 and K_2, and contains η_1 and η_2.

After twinning, the angle between (0001) matrix and (0001) twin is 94° and we can apply Zeners[28] model for crack initiation. It is conceivable that twin boundary performs the function of stable obstacle against the motion of dislocations and dislocations on a slip plane emanated from a Frank-Read source encounter a barrier (twin boundary) where they will pile up exerting considerable pressure on the few of them at the head of line. As the pressure builds up, there are two alternatives, (1) the obstacle will be overcome and slip will continue, (2) the leading dislocations will be forced together to form a crack nucleus. This idea is illustrated diagramatically in Fig. 32.

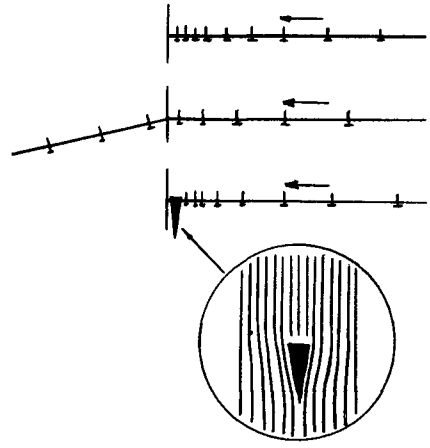

Fig. 32. Zener's Model for the Nucleation of Crack by Dislocation Coalescence as an Alternative to Slip Propagation.

Therefore, if dislocations moving on the (0001) matrix pile up against twin boundary, a wedge-shaped void normal to the (0001) matrix and almost parallel to (0001) twin can be formed. This implies that crack can be nucleated from this void and propagated along (0001) twin (see Fig. 24).

When the exposure time after mercury coating was short (5-15 mins) the crystals failed by Zener type crack initiation. Of course, fracture occurred at less shear strain compared to uncoated crystals because of the shortening of stage A. When the time of exposure in air after mercury coating increased beyond 15 mins., a completely different type of fracture appeared. The fracture plane was the basal plane of matrix crystal and specimens failed in stage A before twins occur. This kind of fracture was also observed in prestrain effect and higher temperature effect experiments. The number of dislocation rings formed by the condensation of vacancies and then stabilized by diffused mercury atoms could be increased under above mentioned experimental conditions. Therefore, it is understandable that these rings act as short-range obstacles against the motion of dislocations.

Gilman and Read[29] have investigated the formation of tensile kink with various shapes of zinc monocrystals. They came to the conclusion that both axial twisting and curvature of the surface resulting from tensile kink can occur if the shear strains due to slipping on a given basal plane are heterogeneous across the basal plane. They also observed that plated films of copper affected the appearance of the surrated surfaces by increasing their intensity. This suggests that the egress of dislocation was disturbed by plated copper films thereby introducing tensile kinks. During the tensile deformation of both coated and uncoated crystals, serrated surfaces with a

series of small tensile kinks were observed and more embryos of tensile kink appeared in coated and longer exposed specimens (see metallographic observations). Interaction between diffused mercury atoms and dislocations or dislocation rings induced heterogeniety in slip process revealing tensile kinks on the surface of crystals. Frequent failure of mercury coated crystals at the kink bands suggest that kink boundary can also be a stable obstacle against dislocation motion (see Fig. 25). Both increased number of stabilized dislocations rings and kink boundaries perform the function of stable obstacle for the pile up of dislocation. In this case, we can apply Bullough - Gilman - Rozhanskii model for crack initiation shown in Fig. 33.

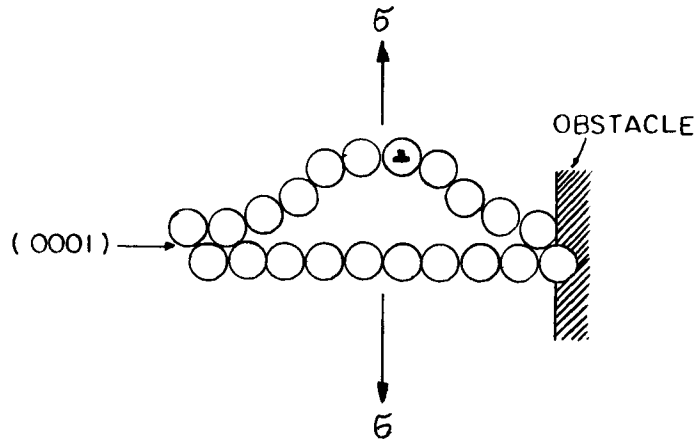

Fig. 33. Schematic of Bullough - Gilman - Rozhanskii Model for Crack Initiation in Zinc.

Under the action of a tensile stress σ , the lattice in the vicinity of a blocked group of dislocations bend about an axis parallel to the basal plane and perpendicular to Burger's vector. If σ is sufficiently large, a cleavage crack may be initiated along the basal plane (see Fig. 26-27).

VI. CONCLUSION

(1) Interaction between diffused surface active liquid metal and obstacles to slip is a prerequisite for embrittlement during tensile deformation of zinc single crystals oriented for single slip.

(2) The possible origins of stable obstacles are considered to be:
   (a) dislocation rings formed by vacancy condensation and stabilized by diffused mercury atoms.
   (b) twin boundaries or tensile kink walls resulting from non-uniform deformation across slip planes due to the restraining of the motion of glide dislocations by short-range obstacles (stabilized dislocation rings).

(3) The modifications of work hardening characteristics of zinc single crystals resulting from mercury coating are summarized to be:
   (a) increase in critical resolved shear stress, and increase of work hardening slope in stage A and stage B.
   (b) decrease in transition strain from stage A to B.
   (c) decrease in fracture stress and fracture strain.

(4) Cracks are initiated at tensile kink walls or twin boundaries. (depend on experimental conditions). Relevant mechanisms for initiation and propagation of cracks are considered to be:
   (a) Zener's model for cracks initiated at twin boundaries.
   (b) Bullough - Gilman - Rozhanskii model for cracks initiated at kink walls.

APPENDIX A

THERMODYNAMICS OF THE SPREADING OF LIQUIDS ON SOLID PHASE[30]

The free energy of a substance, at constant temperature, pressure and concentration is defined as

$$\left(\frac{\partial F}{\partial A}\right)_{P.T.N.} \equiv \gamma = \begin{array}{l}\text{free surface energy per} \\ \text{square centimeter}\end{array} \qquad \ldots\ldots 1$$

where F = the free energy of the substance and A = its surface area. γ is usually expressed in erg per square centimeter or dynes per centimeter. First of all, the condition for spreading to occur is that for the entire system

$$dF < 0 \qquad \ldots\ldots 2$$

It is assumed that in the course of spreading of spreading of liquid b on a surface a, the following area relations are obtained.

$$d A_b = d A_{ab} = -dA_a \qquad \ldots\ldots 3$$

then

$$\left(\frac{\partial F}{\partial A}\right)_{P.T} = \gamma_b + \gamma_{ab} - \gamma_a \qquad \ldots\ldots 4$$

Let $-\left(\frac{\partial F}{\partial A}\right)$ be designed as the final spreading coefficient $S^{b'}/_{a'}$,

then

$$S^{b'}/_{a'} = \gamma_{a'} - (\gamma_{b'} + \gamma_{a'b'}) \qquad \ldots\ldots 5$$

where P,T = constant and the surfaces saturated by the mutual components is designated by the primes. For the specific case at hand, component b is the

liquid and a the solid. We, therefore, redefine the spreading coefficients

$$S^{L}/_{S} = \gamma_{S} - (\gamma_{L} + \gamma_{L'S'}) \quad \text{initial} \quad \ldots\ldots 6$$

$$S^{L'}/_{S} = \gamma_{S} - (\gamma_{L'} + \gamma_{L'S'}) \quad \text{semi-initial} \quad \ldots\ldots 7$$

$$S^{L'}/_{S'} = \gamma_{S'} - (\gamma_{L'} + \gamma_{L'S'}) \quad \text{final} \quad \ldots\ldots 8$$

As a primary guide from the above discussion, we derive that a necessary condition for spreading is

$$\gamma_{S} > \gamma_{L} \quad \ldots\ldots 9$$

APPENDIX B

DISLOCATION PIPE DIFFUSION[25]

The term pipe diffusion, which has frequently been applied to diffusion along dislocation, might well have been coined to represent the line of vacant sites lying under dislocation line. The core of the dislocation may be defined as the last line of filled sites in the inserted plane of an edge dislocation together with the line of vacant sites into which that plane would grow by negative climb. This is illustrated for a simple cubic lattice in Fig. 1. An interstitial in the dislocation core may be defined as an atom in the row of vacant sites in the core: a vacancy, as an empty site in the line of atoms in the core (Fig. 2).

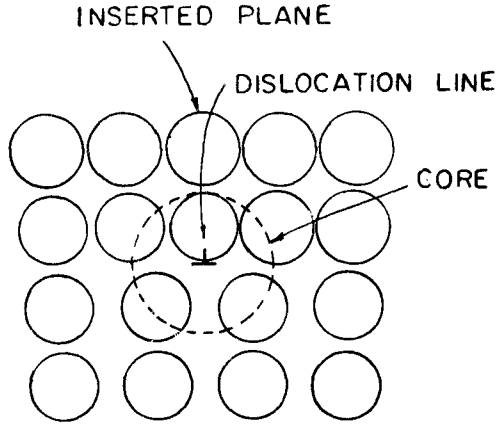

Fig. 1. Pure Edge Dislocation in Simple Cubic Lattice.

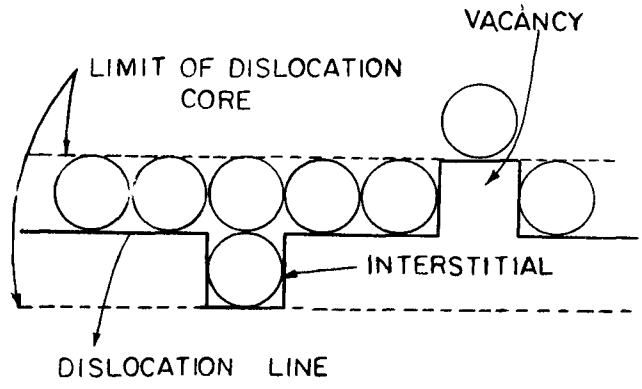

Fig. 2. Illustrating "Interstitial" and "Vacancy" in Pure Edge Dislocation.

Consider a plane constructed perpendicular to the dislocation line and not coincident with a rest position of an interstitial atom in the dislocation. The probability of an atom jumping from left to right across this plane can be written.

$$J_{1\text{-}2} = ac_1\Gamma_T \qquad \ldots\ldots 1$$

Where $J_{1\text{-}2}$ is the flux from left to right across the plane, Γ_T is the jump frequency of an atom in an interstitial position, and ac_1 is the probability that the interstitial site to the left of the reference plane is occupied by a tracer atom (a = lattice parameter). The probability of a jump in the reverse direction across the plane is then given by

$$J_{2\text{-}1} = a\Gamma_T \left(c_1 + a\frac{\partial c_1}{\partial x}\right) \qquad \ldots\ldots 2$$

Where the distance between rest position of interstitial atom is assumed to be a, and $\frac{\partial c_1}{\partial x}$ is the local gradient in interstitial tracer atoms. If the free energy required to create an interstitial atom in the dislocation core is ΔG_i, then the probability of a given site in the core containing an interstitial atoms is

$$p = \exp\left(-\Delta Gi/RT\right) \qquad \ldots\ldots 3$$

The probability that any occupied site contains a tracer atom is simply the local concentration of tracer atom C_o. The combined probability of an interstitial site containing an atom which is also a tracer atom is, then, the product

$$C_1 = C_o \exp\left(-\Delta Gi/RT\right) \qquad \ldots\ldots 4$$

The net tracer flux can be obtained from equations (1), (2) and (4) and is given by

$$J_{net} = -a^2 \Gamma_T \exp(-\Delta Gi/RT) \quad \text{——} \qquad \ldots\ldots 5$$

Comparison of equation 5 with Ficks first law indicates tha

$$D = a^2 \Gamma_T \exp(-\Delta Gi/RT) \qquad \ldots\ldots 6$$

Further Γ_T is simply the product of the vibration frequency of an interstitial atom on the dislocation core, ν and the probability that the atom will acquire sufficient energy to cross the barrier between neighbouring sites. If the barrier between neighbouring sites has height ΔGm, the jump frequency becomes

$$\Gamma_T = \nu \exp(-\Delta Gm/RT) \qquad \ldots\ldots 7$$

and equation 6 may be written

$$D = a^2 \nu \exp[-(\Delta Gi + \Delta Gm)/RT] \qquad \ldots\ldots 8$$

It is assumed that, as soon as an interstitial atom is created and separated from its "parent" vacancy by a single atomic distance, it no longer interacts with that vacancy.

APPENDIX C RESULTS OF TENSILE TEST

Tensile Test Results (specimens with protected end)

Specimen No.	X_o	λ_o	τ_c(Kg/cm²)	Θ_A(Kg/cm²/u.s.)	τ_{A-B}(Kg/cm²)	γ_{A-B}(%)	Θ_B(Kg/cm²/u.s.)	τ_f(Kg/cm²)	γ_f(%)	Experimental Condition
ZXS-X-1	44°	46°	1.71	10.3	19	150	62.5	101.0	413	Non-coated R.T. test.
ZXS-C-3	46°	48°	1.69	11.2	20	140	63.0	102.7	394	Non-coated R.T. test
ZXS-D-3	48°	49°	1.81	10.0	-	-	-	16.2	81	*30% prestrained, coated and 5 min. exposure. R.T. test
ZXS-D-2	48°	49°	1.69	10.3	-	-	-	16.3	91	30% prestrained, coated and 5 min. exposure. R.T. test
ZXI-P-2	46°	48	1.67	11.0	-	-	-	19.2	151	100% prestrained, coated and 5 min. exposure. R.T. test
ZXS-L-2	47°	47°	1.78	13.0	-	-	-	26.2	153	105% prestrained, coated and 5 min. exposure. R.T. test
ZXZ-P-4	46°	48°	1.63	10.3	18	125	-	40.8	184	162% prestrained, coated and 5 min. exposure. R.T. test
ZXI-P-3	46°	48°	1.65	10.0	18	140	-	37.7	191	165% prestrained, coated and 5 min. exposure. R.T. test
ZXI-N-3	44°	46°	2.00	13.3	17	110	95	104.1	304	coated and 5 min. exposure. R.T. test

*8 secs in 50ccHg

Appendix III (cont'd)

Tensile Test Results (specimens with protected end)

Specimen No.	X_o	λ_o	τ_c (Kg/cm²)	θ_A (Kg/cm²/u.s.)	τ_{A-B} (Kg/cm²)	γ_{A-B} (%)	θ_B (Kg/cm²/u.s.)	τ_f (Kg/cm²)	γ_f (%)	Experimental Condition
ZXS-F-3	48°	49°	1.99	17.2	21	95	75	100.0	267	✱ coated and 5 min. exposure. R.T.test
ZXS-F-2	48°	49°	1.95	17.2	22	100	70	97.6	254	coated and 5 min. exposure. R.T.test
ZXI-N-2	44°	46°	2.03	12.0	16	100	95	97.0	267	coated and 10 min. exposure. R.T.test
ZXI-O-4	42°	45°	2.03	16.0	21	90	70	59.0	173	coated and 15 min. exposure. R.T.test
ZXI-O-2	42°	45°	2.06	17.1	22	80	65	61.6	179	coated and 15 min. exposure. R.T.test
ZXI-M-3	42°	44°	2.07	12.6	-	-	-	13.2	62	coated and 30 min. exposure. R.T.test
ZXI-M-2	42°	44°	2.12	14.3	-	-	-	14.5	72	coated and 30 min. exposure. R.T.test
ZXI-L-4	44°	46°	2.12	13.6	-	-	-	8.7	73	coated and 60 min. exposure. R.T.test
ZXI-O-3	42°	45°	2.11	9.7	-	-	-	6.1	38	coated and 60 min. exposure. R.T.test.
ZXI-V-2	46°	47°	2.09	12.0	-	-	-	13.4	86	coated, 5 min. exposure, 5 min in 50°C bath and quench to R.T. R.T. test

✱ 8 secs in 50ccHg

Appendix III (cont'd)

Tensile Test Results (specimens with protected end)

Specimen No.	X_o	λ_o	τ_c(Kg/cm²)	θ_A(Kg/cm²/μ.s.)	τ_{A-B}(Kg/cm²)	γ_{A-B}(%)	θ_B(Kg/cm²/μ.s.)	τ_f(Kg/cm²)	γ_f(%)	Experimental Condition
ZXI-V-3	46°	47°	2.20	11.0	-	-	-	13.2	90	A coated, 5 min. exposure, 5 min. in 50°C bath and quench to R.T. R.T. test
ZXI-W-3	47°	48°	2.30	15.7	-	-	-	7.5	30	coated, 5 min. exposure, 5 min. in 75° bath and quench to R.T. R.T. test
ZXI-V-1	46°	47°	2.24	13.8	-	-	-	9.3	44	coated, 5 min. exposure, 5 min. in 75°C bath and quench to R.T. R.T. test
ZXI-Y-3	48°	49°	2.52	-	-	-	-	4.6	7	coated, 5 min. exposure, 5 min. in 95° bath and quench to R.T. R.T. test
ZXI-Y-2	48°	49°	2.46	-	-	-	-	5.5	10	coated, 5 min. exposure, 5 min. in 95° bath and quench to R.T. R.T. test

A 8 secs in 50ccHg

Appendix III (cont'd)

Results of Tensile Test (specimens with non-protected ends)

Specimen No.	X_o	λ_o	τ_c(Kg/cm²)	θ_A(Kg/cm²/u.s.)	τ_{A-B}(Kg/cm²)	γ_{A-B}(%)	θ_B(Kg/cm²/u.s.)	Experimental Condition
ZXS-K-2	49°	49°	1.76	10.5	19	135	85	non-coated. R.T. test
ZXS-I-2	46°	48°	1.71	10.5	-	-	-	100% prestrained, coated* and 5 min. exposure. R.T. test
ZXS-T-3	46°	48°	1.73	15.3	-	135	-	150% prestrained, coated and 5 min. exposure. R.T. test
ZXS-T-2	46°	48°	1.72	12.0	-	115	65	200% prestrained, coated and 5 min. exposure. R.T. test
ZXS-W-3	44°	46°	1.76	10.0	16	125	86	2 secs in 50ccHg and 5 min. exposure. R.T. test
ZXS-H-2	47°	49	1.75	12.2	23	125	70	2 secs in 50ccHg and 5 min. exposure. R.T. test
ZNX-F-2	47°	48°	1.82	12.0	20	115	50	2 secs in 50ccHg and 5 min. exposure. R.T. test
ZXS-J-1	44°	46°	1.77	10.0	16	115	75	4 secs in 50ccHg and 5 min. exposure. R.T. test
ZXS-G-3	48°	50°	1.79	13.0	20	125	80	4 secs in 50ccHg and 5 min. exposure. R.T. test
ZXII-E-1	47°	48°	1.81	8.5	13	125	60	4 secs in 50ccHg and 5 min. exposure. R.T. test
ZXS-W-2	44°	46°	1.83	11.4	16	110	-	6 secs in 50ccHg and 5 min. exposure. R.T. test

*4 secs in 50ccHg

Appendix III (cont'd)

Results of Tensile Test (specimens with non-protected ends)

Specimen No.	X_o	λ_o	τ_c (Kg/cm^2)	θ_A (Kg/cm^2/u.s.)	τ_{A-B} (Kg/cm^2)	γ_{A-B} (%)	θ_B (Kg/cm^2/u.s.)	Experimental Condition
ZXS-G-1	48°	50°	1.84	11.8	19	115	-	6 secs in 50ccHg and 5 min. exposure. R.T. test
ZXII-E-2	47°	48°	1.82	11.0	17	125	85	6 secs in 50ccHg and 5 min. exposure. R.T. test
ZXS-U-1	43°	45°	1.96	12.3	15	100	-	8 secs in 50ccHg and 5 min. exposure. R.T. test
ZXS-D-1	48°	49°	2.02	12.0	-	-	-	8 secs in 50ccHg and 5 min. exposure. R.T. test
ZXII-B-2	46°	46°	2.03	-	-	-	-	8 secs in 50ccHg and 5 min. exposure. R.T. test

APPENDIX D

ESTIMATION OF ERRORS

Critical resolved shear stress is obtained from the relation

$$\tau_c = \frac{P}{A} \sin X_o \cos\lambda_o \qquad \ldots\ldots 1$$

where P is load, A is initial cross sectional area and X_o and λ_o have the same meaning as defined previously. By taking natural logarithms and differentiating equation (1), the total error involved in calculating critical resolved shear stress is

$$\frac{\delta\tau_c}{\tau_c} = \frac{\delta P}{P} + \frac{\delta A}{A} + \frac{\delta(\sin X_o)}{\sin X_o} + \frac{\delta(\cos\lambda_o)}{\cos\lambda_o} \qquad \ldots\ldots 2$$

The possible uncertainties are:

(1) the load value from the chart, the deviation point from linearity would be determined to within at least 0.2 division in 4, hence

$$\frac{\delta P}{P} = \frac{0.2}{4} = 0.05$$

(2) specimen cross section, the micrometer could be read to 0.001cm in 0.05 cm, hence

$$\frac{\delta A}{A} = \frac{2(0.001)}{0.05} = 0.04$$

(3) the crystal orientation could be determined within ±1° using the Wulff net, hence for $X_o = 46°$

$$\frac{\delta(\sin X_o)}{\sin X_o} = \frac{0.012}{0.719} = 0.017$$

and for $\lambda_o = 46°$

$$\frac{\delta(\cos\lambda_o)}{\cos\lambda_o} = \frac{0.012}{0.695} = 0.017$$

Therefore, total uncertainties involved in critical resolved shear stress is

$$\frac{\delta\tau_c}{\tau_c} = 0.074 \quad \text{or} \quad 7.4\%$$

The flow stress values involve additional parameter, the gage length, variation in cross sectional area along gage section and the amount of mercury coated. Especially, the amount of mercury coated on the surface of crystals depends on the surface condition (degree of micro relief and possible contaminations) and this will affect the parameters defined for comparison but there is no relevant way to estimate the resulting error.

REFERENCES

1. Nichols, H., and Rostoker, W., Acta Met. 9, 504 (1961).

2. Goryunov, U.V., Pertsov, N.V., and Rehbinder, P.A., Soviet Physics "Doklady", 4, 840 (1960).

3. Heyn, E., J. Inst. Metals 12, 3 (1914).

4. Rawdon, H.S., Proc ASTM 18, 2, 189 (1918).

5. Moor, R., and Beckinsale, S., J. Inst. Metals, 23, 225 (1920).

6. Miller, H.J., J. Inst. Metals, 37, 183 (1927).

7. Rosenberg, R., and Cadoff, I., Fracture of Solids, Edited by D.C. Drucker and J.J. Gilman (1962).

8. Likhtman, V.I., and Shchukin, E.D., Soviet Physics "Uspekhi", I.91 (1958).

9. Shchukin, E.D., Perstov, N.V., and Goryunov, U.V., Soviet Physics (Crystallography), 4, 800 (1959).

10. Labzin, V.A. and Likhtman, V.I., "Doklady", Akad Nauk, SSSR 121, 778 (1958).

11. Rehbinder, P.A., Likhtman, V.I., and Kochanova, L.A., "Doklady", Akad Nauk, SSSR 111, 1276 (1956).

12. Likhtman, V.I., Kochanova, L.A., and Bryukhanova, L.S., "Doklady" Akad Nauk, SSSR 120, 757 (1958).

13. Kamdar, M.H., and Westwood, A.R.C., Embrittlement of Zinc Monocrystals and Bicrystals by Mercury and Gallium, RIAS, March (1965).

14. Kamdar, M.H., and Westwood, A.R.C., Concerning Liquid Metal Embrittlement Particularly of Zinc Monocrystals by Mercury, RIAS, Dec. (1962).

15. Perstov, N.V., and Rehbinder, P.A., "Doklady", Akad Nauk, SSSR, 124, 307, (1959).

16. Anderson, E.A., Metals Handbook, (1948).

17. Simson, C.Von., Z. Physik Chem. 109, 192 (1924).

18. Boas, W., An Introduction to the Physics of Metals and Alloys, 67, (1947).

19. Jillson, D.C., Trans. AIME, 188 (1950).

References (cont'd)

20. Harkins, W.D., Physical Chemistry of Surface, Reinhold Pub. Co., N.Y. (1952).

21. Fricke, R., Z. Elektrochem., 52, 72 (1948).

22. Pleteneva, N.A., and Fedoseeva, N.P., "Doklady", Akad Nauk, SSSR 151, 2 (1963).

23. Love, G.R., Acta Met. 12, 6 (1964).

24. Frank, F.C., Mathematical Theory of Stationary Dislocation, Phil. Mag. Suppl., July (1952).

25. Mott, N.F., Phil. Mag. 43 (1952), Phil. Mag. 44 (1953).

26. Seeger, A. Von., and Trable, H., Z. Metalkunde (1960).

27. Hirsch, P.B., Silcox, J., Smallman, R.E., and Westmacott, K.H., Phil. Mag. 3 897, (1958).

28. Zener, C., "Fracturing of Metals", pp.3-31 ASM (1948).

29. Gilman, J.J., Read, T.A., Trans. AIME 194, 875 (1952).

30. Bondi, A., Chem. Rev., 52, 427 (1953).